

Table VII. Intermolecular Contacts (Å) Suggesting Hydrogen Bonding for Complex **1**^a

Cl(1)	O(9)	3.14 (1)	Cl(2)	O(11) ^d	3.25 (1)
Cl(1)	O(10)	3.16 (1)	Cl(2)	O(7) ^e	3.35 (1)
Cl(1)	O(8) ^b	3.20 (1)	Cl(2)	O(7) ^f	3.37 (1)
Cl(1)	O(8)	3.22 (1)	O(9)	O(10) ^b	2.76 (2)
Cl(2)	O(11) ^c	3.19 (1)	O(10)	O(11)	2.83 (2)

^aSymmetry codes are given in footnotes *b-f*. ^b1 - *x*, 1 - *y*, 1/2 + *z*. ^c1 - *x*, 1 - *y*, -1/2 + *z*. ^d-1/2 + *x*, 1 - *y*, *z*. ^e*x*, -1 + *y*, *z*. ^f1/2 - *x*, -1 - *y*, -1/2 + *z*.

A number of important hydrogen bonds would appear to be made between the various water molecules and chloride ions within the crystal lattice (Figure 6); close contacts between heavy atoms which almost certainly are mediated by hydrogen bonds are listed in Table VII. Unfortunately, we were unable to locate the appropriate hydrogens crystallographically, making any detailed discussion of this hydrogen-bonding network inappropriate.

Summary and Conclusions

In the solid state, uncomplexed 18-crown-6 displays an elliptical conformation of *C*₂ symmetry. In solution, although 18-crown-6 is conformationally mobile, some preference for the more symmetrical *D*_{3d} conformation has been noted. Upon complexation with potassium ion, both solution and solid-state studies have

(24) Dobler, M.; Dunitz, J. D.; Seiler, P. *Acta Crystallogr.* 1974, B30, 2741-2743. Dunitz, J. D.; Dobler, M.; Seiler, P.; Phizackerley, R. P. *Acta Crystallogr.* 1974, B30, 2733-2738.

previously demonstrated that 18-crown-6 adopts a more symmetrical *D*_{3d} or near-*D*_{3d} conformation, thus directing all six oxygen donors toward the complexed potassium ion. The unusual complex [(18-crown-6)K(H₂O)₃](H₃O)(H₂O)Cl₂ (**1**) crystallizes from CHCl₃/CH₂Cl₂ solutions of 18-crown-6 and dipotassium tartrate, perhaps a result of deprotonation of solvent by the solubilized tartrate ion. The crown ether in this complex adopts a quite unsymmetrical conformation, with the oxygens disposed in a twist-boat arrangement around the potassium, rather than the symmetrical *D*_{3d} conformation, which places the oxygens in a chair arrangement. The potassium ion in this complex is effectively "shrink-wrapped", with all oxygen-potassium bonds appreciably shorter than in other 18-crown-6 complexes of potassium. The question of what factors are responsible for formation of this unusual crown ether geometry and for the contraction of the bonds in this complex remains an open one, but it is clear that even a prototypical crown ether such as 18-crown-6 may continue to provide unusual and unexpected coordination complexes and geometries.

Acknowledgment. This work was supported by the Office of Naval Research.

Supplementary Material Available: Details of crystallographic data collection and refinement and tables of intermolecular contacts, anisotropic thermal parameters, torsion angles, and calculated positions of hydrogen atoms of **1** (9 pages); observed and calculated structure factors of **1** (9 pages). Ordering information is given on any current masthead page.

Silver, Sodium Halosodalites: Class A Sodalites

Andreas Stein,[†] Geoffrey A. Ozin,^{*,†} Peter M. Macdonald,[†] Galen D. Stucky,[†] and Raz Jelinek[‡]

Contribution from the Lash Miller Chemical Laboratories, University of Toronto, 80 Saint George Street, Toronto, Ontario, Canada, M5S 1A1, Department of Chemistry, University of California, Santa Barbara, California 93106, and Materials Science Division, Lawrence Berkeley Laboratory and the Department of Chemistry, University of California, Berkeley, California 94720. Received October 11, 1991

Abstract: Class A sodalites of the composition Na₈X₂(SiAlO₄)₆ were synthesized hydrothermally (X = Cl⁻, Br⁻, I⁻). AgNO₃ melt and hydrothermal aqueous exchanges were used to replace Na⁺ ions by Ag⁺ ions. The sodalite precursors and products were studied by chemical analysis, powder XRD, mid- and far-IR, multinuclear MAS- and DOR-NMR and optical reflectance spectroscopy. The structures of selected precursors as well as partially and fully silver exchanged sodalites were determined by Rietveld refinement of high resolution powder X-ray data. The unit cell sizes depended on the type and loading of cation and anion. Combined results from the above techniques indicated that a solid-solution structure of cages with different cation contents was formed. Organized assemblies of Na_{4-n}Ag_nX³⁺ clusters consisting of the components of insulators (NaX) and semiconductors (AgX) were encapsulated by the cubic sodalite framework which forms perfectly periodic arrays of all-space filling 6.6 Å cages. The concentration and identity of cations and nature of the anion controlled the extent of vibrational and electronic coupling between clusters. Vibrational coupling was strongly mediated by the anions. Electronic interaction was possible through the framework (Na, Ag) or directly (Ag). Extended Hückel molecular orbital calculations supported the idea of band formation for an extended Na_{4-n}Ag_nX³⁺ cluster lattice at increasing Ag⁺ loadings. They also aided in the assignment of the optical spectra. The calculations indicated that electronic transitions existed between clusters and the framework.

Introduction

Traditional or previously suggested applications of sodalites have included pigments, gas storage materials, and the use of photochromic and cathodochromic sodalites for information storage,

display, and filter optics.¹ Because sodalites allow one to create organized assemblies of clusters consisting of the components of insulators, semiconductors, or metals, inside a host material composed of single size bcc packed cuboctahedral cavities,²⁻⁴ new

[†] University of Toronto.

[‡] University of California, Santa Barbara.

[§] University of California, Berkeley.

(1) Stein, A.; Ozin, G. A Sodalite: An Old Material for Advanced Uses. In *Advances in the Synthesis and Reactivity of Solids*; Mallouk, T. E., Ed.; 1991; Vol. 3, and references cited therein.

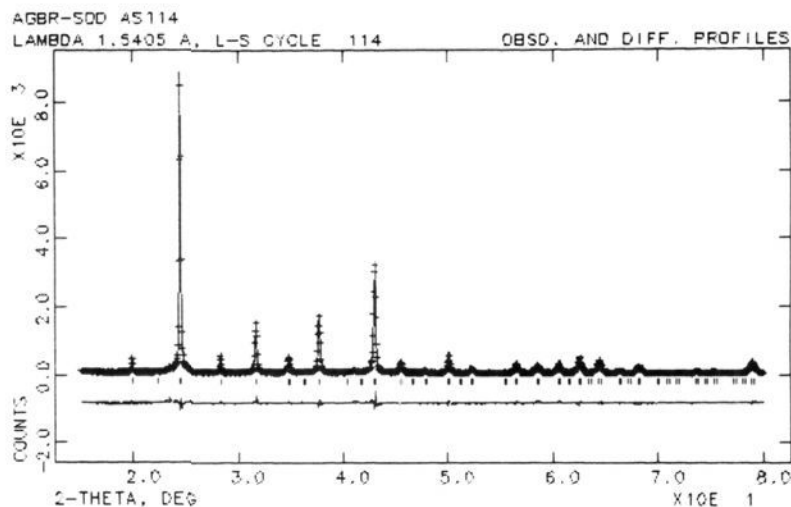


Figure 1. High resolution XRD powder pattern of AgBr-SOD, showing the experimental pattern, superimposed on a pattern calculated by Rietveld refinement, and the difference between these two patterns.

applications for sodalites would be based on the confinement of small clusters in organized arrays. These could include, for example, waveguides, nonlinear optical materials, optical computing, and quantum electronics.

In ideal class A sodalites,^{2a} each cage is filled with an M_nX or $M_nN_{4-n}X$ ($n = 0-4$) cluster, where M and N refer to monovalent cations, such as Na^+ or Ag^+ , and X is one of the halides (Cl^- , Br^- , I^-). This paper reports details of the structural, electronic, and optical properties of class A sodalites.

Rietveld Structure

Rietveld methodology was used to successfully refine many of the sodalite structures presented in this study. The success with sodalites can be partially attributed to the relatively simple, highly symmetric, static structure of sodalites that yields diffraction patterns with minimal peak overlap.⁵ A typical example of an observed powder pattern, a pattern calculated by Rietveld refinement and the difference between the two is shown in Figure 1. Pauling's structure of sodium chlorosodalite⁶ and more recent sodalite refinements⁷⁻⁹ provided suitable starting models. The reader is referred to several good recent reviews of Rietveld methods.¹⁰⁻¹³

The crystal structure of NaCl-SOD was first solved by Pauling in 1930.⁶ Since then structures have been determined by refinement or calculation for the following sodalites: LiCl-SOD,^{14,15}

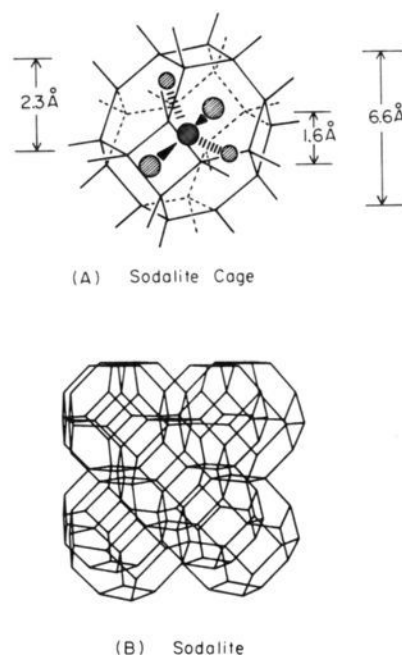


Figure 2. A. Sodalite cage showing a single cuboctahedron, a central anion, and four cations in the six-ring sites. Each corner represents a TO_4 unit ($T = Si$ or Al). B. Sodalite framework, emphasizing the bcc close packing of cages.¹¹⁰

NaCl-SOD,^{7,9,14-17} KCl-SOD,¹⁴ NaBr-SOD,^{16,17} NaI-SOD,^{14,16,17} NaOH-SOD,^{8,18} Na[]-SOD^{19,20} as well as for the related compounds nosean,²¹ lazurite,²² a gallium sodalite,²³ silica sodalite,²⁴ and a number of aluminated sodalites.²⁵⁻²⁷ Class A sodalites have

- (2) (a) Stein, A.; Ozin, G. A.; Stucky, G. D. *J. Am. Chem. Soc.* **1990**, *112*, 904-905. (b) Stein, A.; Macdonald, P. M.; Ozin, G. A.; Stucky, G. D. *J. Phys. Chem.* **1990**, *94*, 6943-6948. (c) Stein, A.; Meszaros, M.; Macdonald, P. M.; Ozin, G. A.; Stucky, G. D. *Adv. Mater.* **1991**, *3*, 306-309. (d) Stein, A.; Ozin, G. A.; Stucky, G. D. *J. Soc. Photogr. Sci. Technol. Japan* **1990**, *53*, 322-328.
- (3) Ozin, G. A.; Kuperman, A.; Stein, A. *Angew. Chem.* **1989**, *101*, 373-90.
- (4) Ozin, G. A.; Kirkby, S.; Meszaros, M.; Özkaz, S.; Stein, A.; Stucky, G. D. In *Materials for Nonlinear Optics: Chemical Perspectives*, Marder, S. R., Sohn, J. E., Stucky, G. D., Eds.; *A.C.S. Symp. Ser.* **1991**, *455*, 555-581.
- (5) Post, J. E.; Bish, D. L. in ref 13, pp 277-305.
- (6) Pauling, L. *Proc. Natl. Acad. Sci. U.S.A.* **1930**, *16*, 453. Pauling, L. *Kristallogr.* **1930**, *74*, 213.
- (7) Löns, J.; Schulz, H. *Acta Crystallogr.* **1967**, *23*, 434.
- (8) Hassan, I.; Grundy, H. D. *Acta Crystallogr.* **1983**, *C39*, 3-5.
- (9) Hassan, I.; Grundy, H. D. *Acta Crystallogr.* **1984**, *B40*, 6-13.
- (10) Albinati, A.; Willis, B. T. M. *J. Appl. Cryst.* **1982**, *15*, 361-374.
- (11) Baerlocher, Ch. *Zeolites* **1986**, *6*, 325-333.
- (12) Larson, A. C.; Von Dreele, R. B. *Generalized Structure Analysis System*; LANSCE, MS-H805, Los Alamos National Laboratory, Los Alamos, NM 87545, 1988.
- (13) Modern Powder Diffraction. Bish, D. L., Post, J. E. Eds.; *Rev. Mineralogy* **1989**, *20*.
- (14) Beagley, B.; Henderson, C. M. B.; Taylor, D. *Mineral. Mag.* **1982**, *56*, 459-464.
- (15) Weller, M. T.; Wong, G. *Solid State Ionics* **1989**, *32/33*, 430-435.
- (16) Henderson, C. M. B.; Taylor, D. *Phys. Chem. Mineral.* **1978**, *2*, 337.

- (17) Dempsey, M. J.; Taylor, D. *Phys. Chem. Miner.* **1980**, *6*, 197-208.
- (18) Luger, S.; Felsche, J.; Fischer, P. *Acta Crystallogr.* **1987**, *C43*, 1-3.
- (19) Felsche, J.; Luger, S.; Baerlocher, Ch. *Zeolites* **1986**, *6*, 367-372.
- (20) Felsche, J.; Luger, S.; Fischer, P. *Acta Crystallogr.* **1987**, *C43*, 809-811.
- (21) Hassan, I.; Grundy, H. D. *Can. Mineral.* **1989**, *27*, 165-172.
- (22) Hassan, I.; Peterson, R. C.; Grundy, H. D. *Acta Crystallogr.* **1985**, *C41*, 827-832.
- (23) McCusker, L. B.; Meier, W. M.; Suzuki, K.; Shin, S. *Zeolites* **1986**, *6*, 388.
- (24) Richardson, J. W.; Pluth, J. J.; Smith, J. V.; Dytrych, W. J.; Bibby, D. M. *J. Phys. Chem.* **1988**, *92*, 243-247.
- (25) Depmeier, W. *Acta Crystallogr.* **1984**, *C40*, 226. Depmeier, W. *J. Appl. Cryst.* **1979**, *12*, 623.
- (26) Depmeier, W.; Schmid, H.; Setter, N.; Werk, M. L. *Acta Crystallogr.* **1987**, *C43*, 2251.

Table I. Structural Parameters of Class A Sodalites

sample	ref	uc edge (Å)	∠Al-O-Si (deg)	Al-O (Å)	Si-O (Å)	Ag-X (Å)	Na-X (Å)
AgCl-SOD	own	8.8708	140.6	1.711	1.620	2.537	
AgBr-SOD	own	8.9109	141.7	1.705	1.630	2.671	
AgI-SOD	own	8.9523	151.4	1.697	1.569	2.779	
NaCl-SOD	14	8.879	138.4	1.766	1.592		2.691
NaCl-SOD	15	8.8812	138.1				2.734
NaCl-SOD	15	8.8812	138.1				2.734
NaBr-SOD	own	8.9305	140.6	1.734	1.620		2.888
NaI-SOD	14	9.008	145.3				3.089
LiCl-SOD	15	8.4440	124.5			2.557Li	
LiCl-SOD	14	8.447	125.6	1.739	1.619	2.451Li	
Li _{3.85} Na _{4.15} Cl-SOD	15	8.7101	132.1			2.835Li	2.527
K _{7.6} Na _{0.4} Cl-SOD	14	9.253	155.4	1.82	1.53	3.007K	
Na _{7.7} Ag _{0.3} Br-SOD	own	8.9290	139.9	1.735	1.626	2.21	2.940
Na _{5.5} Ag _{2.5} Br-SOD	own	8.9123	146.9	1.684	1.603	2.519	2.951

the composition $M_{8-2n}N_{2n}X_2$ -SOD, where X = Cl⁻, Br⁻, or I⁻ and M, N are monovalent cations (Na⁺, Ag⁺). These structures are based on the NaCl-SOD archetype. Having a charge of -3, each sodalite cage contains an anion at its center and four monovalent cations tetrahedrally disposed around it. The cations are 4-fold coordinated, being within bonding distance to the halide ion and three framework oxygens. Figure 2 shows an individual sodalite cage with an M_4X^{3+} cluster. The coordinates, fractional occupancies, isothermal temperature factors, and selected bond lengths, obtained from Rietveld refinements of the silver sodalites, are provided as supplementary material. All sodalite structures studied here were refined using NaCl-SOD with space group $P\bar{4}3n$ as an archetype and starting point. Table I lists the structural parameters of class A sodalites.

Framework. The sodalite framework consists of alternating AlO_4^- and SiO_4 units with a Si/Al ratio of 1 (typically determined as 0.98–1.11 by chemical analysis). These tetrahedral units form a cuboctahedral cage composed of eight six-rings and six four-rings. The Si and Al atoms of a given ring are coplanar. The O atoms alternate above and below the plane. The Si and Al atoms occupy special positions (Wyckoff sites (c) and (d) in the $P\bar{4}3n$ space group no. 218),²⁸ while the O atoms lie on general positions (Wyckoff sites (i)). A reduction in the Al-O-Si angle tends to displace the framework oxygen toward the center of the sodalite cage (decreasing oxygen y -value).

The oxygen x - and z -coordinates are similar in magnitude yet different enough from each other to indicate that the Si and Al atoms are ordered. This agrees with results of ²⁹Si NMR that showed only one Si resonance. In a sample with Si/Al disorder one would expect the oxygen x - and z -coordinates to be identical, which would lead to the space group $I\bar{4}3m$. This was used by Beagley et al. to refine NaI-SOD.¹⁴

The Al-O and Si-O distances fell in the ranges from 1.70–1.74 Å and 1.57–1.63 Å, respectively, i.e., in the usual ranges of bond distances reported for sodalites (e.g., for sodalite Al-O = 1.742 Å, Si-O = 1.620 Å).⁹ Weller and Wong²⁹ noted variations in the Si-O bond length of a series of sodalites, from 1.63 to 1.67 Å. The O-Al-O and O-Si-O angles deviate only slightly from the tetrahedral angle, by ca. $\pm 5^\circ$. For a fully expanded framework composed of ideal tetrahedra the Al-O-Si angle should be 160.5° .³⁰ In the class A sodalites synthesized in this study the Al-O-Si angle varied from 138 to 151° . For the alkali halosodalite series this angle typically increases with the unit cell size¹⁵ (e.g., in the series LiCl-SOD/NaCl-SOD/KCl-SOD: $a_0 = 8.44/8.88/9.25$ Å, $\alpha = 125/138/155^\circ$; or for NaCl-SOD/NaBr-SOD/NaI-SOD: $a_0 = 8.88/8.93/9.01$ Å, $\alpha = 138/141/145^\circ$), although there is no strict correlation between these two parameters when silver and sodium sodalites are compared (e.g., for NaCl-SOD/AgCl-SOD: $a_0 = 8.88/8.87$ Å, $\alpha =$

$138.1/140.6^\circ$; or for NaI-SOD/AgI-SOD: $a_0 = 9.01/8.95$ Å, $\alpha = 145/151^\circ$; or for NaBr-SOD/AgBr-SOD: $a_0 = 8.93/8.87$ Å, $\alpha = 140.6/140.6^\circ$).

On the basis of a geometrical sodalite model,⁹ the unit cell edge theoretically ranges from 8.141 to 9.317 Å. It depends on the identity, size, and number of extraframework constituents as well as on the temperature.¹⁶ Henderson and Taylor³¹ derived empirical formulas relating the cell edges of aluminosilicate sodalites to the mean sizes of the cavity cations and anions. The dependence of the lattice dimension on the anion radius is demonstrated by the cell edges for sodium chloro-, bromo-, and iodosodalites ($a = 8.880$ (3), 8.936 (3), and 9.011 (3) Å, respectively).³² The cell edge increases with increasing average radius of the cage anions. The variation of lattice parameters can be explained by taking into account that the flexible sodalite framework adapts itself to the sizes and to the shapes of the cage ions.³³

The flexibility of the sodalite framework arises from the fact that TO_4 tetrahedra can be tilted by cooperative rotations about the $\bar{4}$ axes, which results in bending of the Si-O-Al angles.^{25,27,34} Depmeier distinguishes between isotropic folding, where the tilt angle has the same absolute value for all tetrahedra and noncubic anisotropic folding which occurs in some aluminate sodalites.²⁵ Tetrahedron-edge-length distortions provide a further means of releasing strains imposed by geometrical constraints. According to Depmeier³⁰ the extent of distortion rises with the aluminum content in a series of aluminosilicate frameworks. The ring openings depend on the T-O-T angles³⁵ as well as on the rotation³⁶ or tilt of the TO_4 building units.³⁰ An increase in temperature also causes an expansion of the unit cell and the ring dimensions.

The unit cell size of class A sodalites varies with the type of halide and the types and relative concentrations of cations present, Table I. The halide effect is mainly a space-filling effect, the large anion causing an expansion of the sodalite cage.

Replacement of Na⁺ by Ag⁺ causes a contraction of the cage. Figure 3 shows that in a series of sodium, silver bromosodalites the unit-cell size decreased slightly as the silver concentration was increased, forming a tighter, more covalent bond between the guest cation and the central anion (four-coordinate $r(Na^+) = 1.13$ Å, $r(Ag^+) = 1.14$ Å).³⁷ At silver concentrations for which most cages contained at least one Ag⁺ ion (at loading levels greater than 2.5–3 Ag⁺/uc) additional silver resulted in weakening of the Ag-X bond, preventing further contraction of the unit cell. Abrupt changes or discontinuities can be observed in unit cell size versus composition plots at certain compositions if either a change in symmetry of the solid solutions or a change in the solid solution mechanism occurs.³⁸ Taking into consideration that Setter and

(31) Henderson, C. M. B.; Taylor, D. *Spectrochim. Acta* 1977, 33A, 283.(32) Hodgson, W. C.; Brinen, J. S.; Williams, E. G. *J. Chem. Phys.* 1967, 47, 3719.(33) Setter, N.; Depmeier, W. *Ferroelectrics* 1984, 56, 45–48; 49–52.(34) Li, Z.; Nevitt, M. V.; Ghose, S. *Appl. Phys. Lett.* 1989, 55, 1730–1731.(35) Taylor, D. *Contrib. Mineral. Petrol.* 1975, 51, 39.(36) Taylor, D. *Mineral. Mag.* 1972, 38, 593.(37) Shannon, R. D. *Acta Crystallogr.* 1976, A32, 751–767.(27) Depmeier, W. *Phys. Chem. Minerals* 1988, 15, 419–426.(28) *International Tables for Crystallography*; Hahn, T., Ed.; D. Reidel Publishing Company: Dordrecht, Holland, 1983; Vol. A.(29) Weller, M. T.; Wong, G. *J. Chem. Soc., Chem. Commun.* 1988, 1103–1104.(30) Depmeier, W. *Acta Crystallogr.* 1984, B40, 185–191.

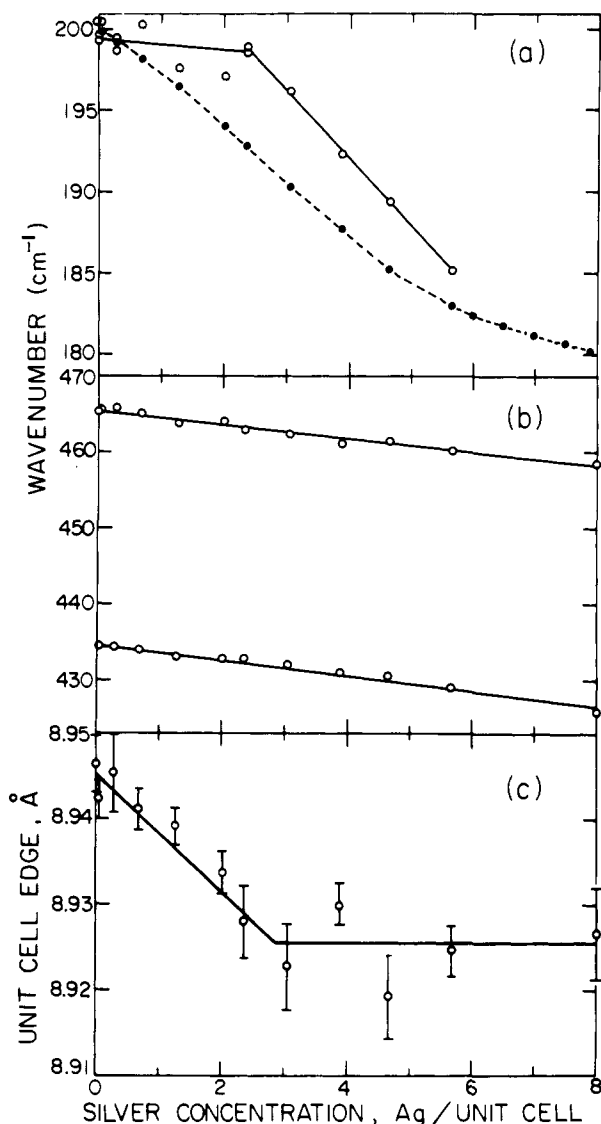


Figure 3. Effect of silver loading on structural and spectroscopic properties of NaAgBr-SOD. (a) Variations in far-IR Na⁺ translational frequencies with Ag⁺ loading (—, untreated samples; --, simulated peak positions assuming a binomial distribution of Na_nAg_{4-n}Br moieties with absorption frequencies centered around equally spaced positions between the $n = 0-4$ extrema). (b) Variations in the mid-IR framework vibrations. (c) Variations in the unit cell edge.

Depmeier³³ observed an almost linear increase in the unit cell edge with average ionic radius of the cage cations and that the Na⁺ and Ag⁺ ions have virtually identical radii, the observed behavior is best explained by considering the more covalent bonding of Ag⁺ with the central halide. This strong interaction results in shortening of the Ag-X distances compared to NaX and an increase in the Ag-O (framework) separations. One is therefore justified in calling a sodalite-encapsulated Ag₄X³⁺ unit a cluster, in spite of its interaction with the framework.

It is interesting to note, that at loading levels near 2.5-3 Ag⁺/uc an abrupt break in magnitude occurred not only for the unit cell edges of the cubic sodalite cage but also for the peak positions of far-IR absorptions associated with a translational mode of Na⁺ near the sodalite six-ring site,³⁹ Figure 3. Both effects may be related to a percolation threshold for connectivity between AgBr units. The unit cell size effect has been described above. In the case of Na⁺ far-IR absorptions, at lower concentrations the

translatory frequency remains essentially constant but decreases at higher concentrations when the proportion of cages containing more than one Ag⁺ increases. Our present hypothesis is that at low concentrations the AgBr molecules act as isolated defects having no effect on the Na⁺ translatory vibrations. Above percolation threshold loadings the Ag⁺ ions must be considered part of the whole unit cell for the vibrational problem and, because of their weaker interaction with the support compared to sodium, reduce the vibrational frequency of the Na⁺ modes. In contrast to the translational modes in the far-IR, the frequency of the aluminosilicate framework vibrations (mid-IR) varies linearly with the silver concentration, see Figure 3.

Anion and Cation Guests. The halide anion has approximately spherical symmetry and always occupies the center of the cage. (In contrast, in NaOH-SOD, a class B sodalite, the OH⁻ is at the center only in the dehydrated sodalite but shifts away from this position after the introduction of the first H₂O molecule into the cavity.⁴⁰) Judging from the isothermal temperature factors, its vibration encompasses an amplitude of ca. ±0.2 Å (for NaCl-SOD $\sqrt{U_{iso}} = 0.155-0.165$ Å, for NaBr-SOD $\sqrt{U_{iso}} = 0.220$ Å, for AgCl-SOD $\sqrt{U_{iso}} = 0.168$ Å, for AgBr-SOD $\sqrt{U_{iso}} = 0.162$ Å, for AgI $\sqrt{U_{iso}} = 0.190$ Å). (Note that $U_{iso} = \bar{U}^2$ is the mean square displacement from the equilibrium position, i.e., the mean square amplitude of the atomic vibration in Å².)

The cation is placed at a 3-fold axis near half of the sodalite six-rings at an $x = y = z$ position. The location $x = y = z = 0.25$ is at the center of the six-ring. In class A sodalites x varies from 0.165 (AgCl-SOD) to 0.198 (NaI-SOD), following the order AgCl-SOD < AgBr-SOD < LiCl-SOD < NaCl-SOD < AgI-SOD < NaBr-SOD < KCl-SOD < NaI-SOD. As the radius of the halide increases, the cation is placed relatively closer toward the six-ring (spatial effect). For a given halide, sodium ions tend to be closer to the six-ring than silver ions. The larger potassium ion moves even closer to the six-ring, at the same time "forcing" the six-ring atoms apart, thus yielding a larger unit cell.

The amplitudes of atomic vibration ($\sqrt{U_{iso}}$) for Ag fell in the range 0.169, 0.163, and 0.150 Å for Cl, Br, and I, respectively. They were lower (0.141 Å) for Br at low Ag loadings. The results imply that in AgI-SOD the Ag⁺ ion vibrates less, as it is more tightly locked into its position (spatial restraint). In the case of the samples with low Ag loading, the Ag⁺ is more highly associated with the Br anion and vibrates less. The fact that U_{iso} is high for Br in these samples simply means that most of the Br anions behave like Br in NaBr-SOD (which also has a high U_{iso} value), and that these Br's dominate. (Note that only the average U_{iso} values were calculated for Br in mixed sodium/silver samples.) The Br associated with Ag may still be relatively less mobile.

Table II lists the cation-anion, cation-oxygen, and silver-silver distances in halosodalites, in addition to theoretical values³⁷ as well as bond lengths in bulk and gas phase silver halides. The silver halide distances inside the sodalite fall between those of the vapor phase molecules and the bulk semiconductor solids. In fully Ag-exchanged halosodalites the Ag-X distances are ca. 8% shorter than in the rock salt bulk materials. Silver-halogen bond lengths for related clusters also appear in Table II. The AgI distances in AgI-SOD compare remarkably well with other cluster species as well as with bulk Ag-I species. The sodalite framework appears to have very little effect on the structure of this cluster. It is notable that, even outside a sodalite cage, Ag₄I³⁺ is claimed to have high stability.⁴¹ For the sodium halosodalites, the bond lengths are only slightly shorter than in the rock salt structures. The distance between silver and a halide anion in the same cage increases on going from Cl and Br to I, while the separation of the silver to an anion in an adjacent cage increases on going through the halide group.

The silver-oxygen distances in these sodalites are slightly longer than typical silver-oxygen separations for four-coordinate silver and significantly longer than those found in two-coordinate silver

(38) Kittel, C. *Introduction to Solid State Physics*, 5th ed.; John Wiley and Sons: New York, 1976.

(39) Godber, J.; Ozin, G. A. *J. Phys. Chem.* **1988**, *92*, 2841-2849, 4980-4987.

(40) Denks, V. P. *Trudy Instituta Fizika Akad. Nauk Estonskoi SSR* **1984**, *55*, 14-71.

(41) Holmberg, B. *Acta Chem. Scand.* **1976**, *A30*, 797-807.

Table II. Interatomic Distances in Class A Sodalites^a

sample	M-X	M-O	Ag-Ag	Ag-Ag (next)	M-X (sum of radii)	M-X (bulk)	Ag-X (mol.)	Ag-X ^b (next)
NaCl-SOD	2.734	2.372			1.13 + 1.67	2.82		
AgCl-SOD	2.537	2.475	4.142	4.920	1.14 + 1.67	2.775	2.28	5.146
NaBr-SOD	2.888	2.356			1.13 + 1.82	2.989		
AgBr-SOD	2.671	2.444	4.361	4.859	1.14 + 1.82	2.887	2.393	5.047
NaI-SOD	3.089	2.383			1.13 + 2.06			
AgI-SOD	2.779	2.576	4.539	4.821	1.14 + 2.06	3.04	2.545	4.918

^aNote: All distances are given in Å. The radii for Na⁺, Ag⁺ are for the four-coordinate cation, while those for Cl⁻, Br⁻, I⁻ are for the six-coordinate anion.³⁷ The bulk Ag-X distances for AgI refer to the zinc-blende structure. ^bRefers to the distance between Ag in one cage and Br in the next cage.

(such as the linear O-Ag-O chain of crystalline Ag₂O (2.04 Å)), see Table II.

The Ag-Ag distances within each cage increase from Cl to Br to I and cover the range from 4.14 to 4.54 Å. Ag-Ag separations for the closest silver ions in adjacent cages are not much larger. These distances decrease from Cl to Br to I. The intracage Ag-Ag separations are ca. 6% longer than in the salts and Ag-Ag distances between cages are from 25% to 12% longer. The Ag-Ag distances in the intrasodalite Ag₄I³⁺ cluster compare closely with those found in related clusters, such as solvated Ag₄I³⁺ (4.6 Å)⁴² and the Ag₄I₆²⁻ cluster, where Ag atoms are also arranged tetrahedrally (4.55 Å). Further Ag-Ag distances are listed in Table II. Extended Hückel molecular orbital (EHMO) calculations (see later) have shown that the orbital overlap, and thus the atomic interaction, is significant for silver at these distances (even though the Ag-Ag separations are much larger than in the metal). One can therefore expect electronic interaction between clusters, as will be shown below. Taking all these bond lengths into account, one can consider the Ag₄X units as expanded silver halide semiconductors, although they are influenced by the aluminosilicate host matrix.

The Rietveld refinement of NaAgBr-SOD containing a very low Ag concentration of 0.3 Ag⁺ per unit cell (uc) yielded an Ag-Br bond length of 2.21 Å. A relatively large isothermal temperature factor for the bromide ion of 0.052 Å² indicates that the anion may be slightly displaced from the center of the cage. After correction for the thermal ion motion,⁴³ the mean separation of Ag and Br falls in the range of 2.21–2.24 Å. A more extreme view, based on three standard deviations, yields a range from 2.0 to 2.4 Å. This distance compares with the internuclear separation of gaseous AgBr (2.39 Å).⁴⁴ The Na-Br distance in this sodalite is 2.94 Å, i.e., slightly longer than in pure NaBr-SOD and only 2% shorter than in the salt. Due to the more extensive covalent bonding of AgBr compared to NaBr, the silver is more closely associated with the halide, while Na⁺ remains more strongly coordinated to the framework oxygen. This results in the Na₃AgBr aggregate behaving more like a slightly perturbed AgBr molecule. On the basis of a binomial distribution of Na_nAg_{4-n}Br moieties, at the silver loading level of this sample one in every eight cages is occupied with an AgBr molecule. The connectivity of AgBr molecules between cages is therefore small, and the AgBr molecules can be considered isolated.

At a slightly higher silver concentration (2.5 Ag/uc) the AgBr distance (2.519 (5) Å) has a value intermediate between the isolated molecule and the fully Ag-loaded sample. This value may in fact be an average of bond lengths for Ag₄Br, Ag₃NaBr, Ag₂Na₂Br, and AgNa₃Br clusters which could not be resolved into individual lengths by the method used.

A word of caution should be given for the last two results, where both the occupancy of the silver ion is quite low, and the separation between the silver and the sodium cations is very small. For a scan to 100°2θ (or 80°2θ) the maximum theoretical resolution was 1.0 Å (or 1.2 Å). In the above mixed sodium, silver sodalites the separation between cation sites is 0.25–0.42 Å, i.e., smaller

than the resolution and approaching the range of the thermal vibrations. However, including both sites improved the *R*-factor over leaving one site out. The fact that the cation of lower occupancy (silver) is a much stronger scatterer than sodium played to our advantage. In a similar situation, Cheetham⁴⁵ mentions the refinement of GeO₂·9Nb₂O₅, where nonstoichiometry was introduced by partial occupancy of a new type of interstitial site (occupancy only 0.10). This site was detected by the Fourier analysis of X-ray data of a single crystal but was not found by powder data. Nevertheless, including the site in the powder refinement brought the *R*-factor down from 10.7 to 9.8%.

Silver Distribution

Regarding the arrangement of silver in sodalites containing both silver and sodium ions, several models can be proposed.⁴⁶ The silver may tend to segregate from the sodium ions and form small domains connected through adjacent cages within the crystal. Hassan and Grundy⁹ proposed this segregation, or domain, model for Na₄K₄Cl-SOD. Another model assumes an even distribution of cations throughout the whole crystal, forming an ordered array of Na_{4-n}Ag_nX³⁺ (for a fixed value of *n*). If clusters have different stability constants for each *n*, the most stable configuration will tend to dominate and therefore influence the distribution. A third possibility is that the distribution remains statistical, for example, following a binomial model. Some cages may be filled with four silver ions, others with one silver and three sodium ions, etc.

It was shown by IR and XRD techniques, by the absence of any splitting or unusual broadening of IR bands or X-ray lines, that partially silver-exchanged products are different from physical mixtures of pure sodium sodalites and pure silver sodalites. This implies that the Na⁺ and Ag⁺ ions are distributed more intimately than in physical mixtures and do not tend to aggregate in specific regions within the matrix. The absence of superlattice reflections in the XRD eliminates the ordered model. In order to be resolved as separate phases by XRD, segregated domains would require a size of at least 20–100 Å. Together, these results suggest that the β-cage encapsulated Na_{4-n}Ag_nX³⁺ moieties follow a statistical distribution, which is solid-solution-like.

Composition

The chemical analyses of the silver sodalites are summarized in Table III. One important factor during the ion exchange is control over the silver loading. Elemental analysis of NaAgBr-sodalites confirmed that at all stoichiometric levels the silver exchange was complete, i.e., virtually all silver present in the reaction mixture was exchanged into the sodalite. With a slight excess of silver nitrate complete replacement of Na⁺ by Ag⁺ was accomplished for all sodalites in one exchange reaction at 230 °C within 20 h. Partial exchange was possible by employing smaller amounts of silver nitrate.

Mid- and Far-Infrared (IR) Spectroscopy

The silver ion exchange process is conveniently monitored by intensity changes of diagnostic sodium and silver ion absorptions in the far-IR as well as shifts in the frequencies of far-IR anion

(42) Yamaguchi, T.; Johansson, G.; Holmberg, B.; Maeda, M.; Ohtaki, H. *Acta Chem. Scand.* **1984**, *A38*, 437–451.

(43) Busing, W. R.; Levy, H. A. *Acta Crystallogr.* **1964**, *17*, 142–146.

(44) Krisher, L. C.; Norris, W. G. *J. Chem. Phys.* **1966**, *44*, 974–976.

(45) Cheetham, A. K.; Taylor, J. C. *J. Solid State Chem.* **1977**, *21*, 253–275.

(46) Ryoo, R.; Liu, S.-B.; de Menorval, L. C.; Takegoshi, K.; Chmelka, B.; Trecocke, M.; Pines, A. *J. Phys. Chem.* **1987**, *91*, 6575.

Table III. Sodalite Compositions

sample	class A sodalites (Chemical Anal.) ^a %					ppmFe	Si/Al
	Na	Ag	Br	Si	Al		
NaBr-SOD	16.27	0.00	13.70	16.17	15.03	47	1.03
NaAgBr-SOD	16.46	0.49	12.98	15.99	14.74	48	1.04
NaAgBr-SOD	15.74	2.72	12.37	15.57	14.33	51	1.04
NaAgBr-SOD	13.97	6.20	11.68	14.59	13.44	52	1.04
NaAgBr-SOD	12.52	11.39	11.49	14.28	13.10	44	1.05
NaAgBr-SOD	11.08	17.17	11.27	13.72	12.44	45	1.06
NaAgBr-SOD	9.19	19.33	10.33	13.21	11.95	41	1.06
NaAgBr-SOD	7.67	23.81	9.55	12.64	11.29	42	1.08
NaAgBr-SOD	6.39	29.31	9.08	12.33	10.82	42	1.09
NaAgBr-SOD	5.29	33.85	9.02	11.89	10.41	46	1.10
NaAgBr-SOD	3.95	37.76	9.28	10.94	9.50	46	1.11
AgBr-SOD	0.04	50.51	8.01	9.76	8.56	37	1.10

^a Samples dehydrated under vacuum at 500 °C for 1 h. The oxygen content exists mainly as framework oxide, with a small amount present as β -cage OH⁻/H₂O.

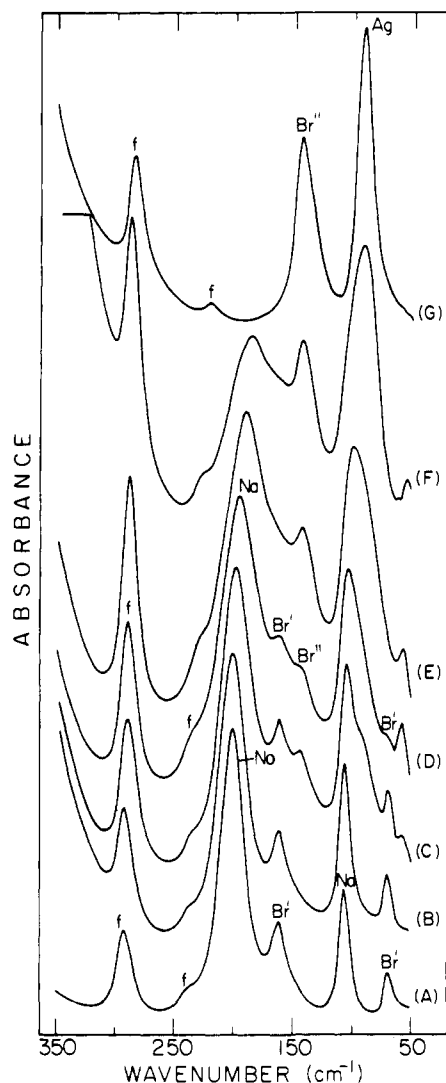


Figure 4. Far-IR spectra of sodium, silver bromosodalites with various silver loadings, showing the silver, sodium and bromide translational modes: (A) 0 Ag/uc, (B) 0.3 Ag/uc, (C) 2.4 Ag/uc, (D) 3.1 Ag/uc, (E) 4.7 Ag/uc, (F) 5.7 Ag/uc, and (G) 8 Ag/uc. "f" denotes a framework absorption.

vibrations.⁴⁷ This technique is capable of directly probing the site occupancy, population, and local environment of exchangeable cations as well as other zeolite framework motions in the 250–500-cm⁻¹ region.⁴⁸ Figure 4 shows far-IR spectra of bromoso-

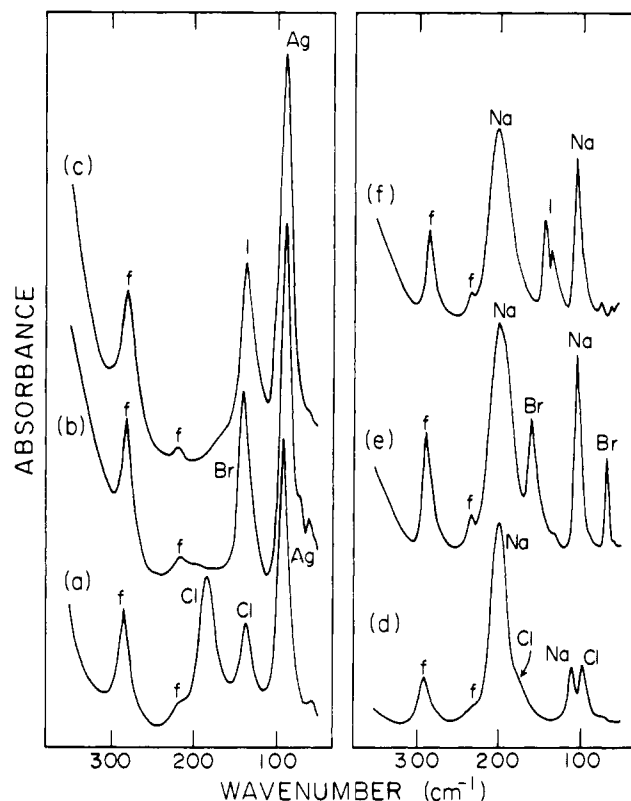


Figure 5. Far-IR spectra of halosodalites: (a) AgCl-SOD, (b) AgBr-SOD, (c) AgI-SOD, (d) NaCl-SOD, (e) NaBr-SOD, and (f) NaI-SOD. "f" denotes a framework absorption.

dalites with increasing replacement of sodium ions by silver. The extent of exchange was followed by comparing the relative intensities of the Na⁺ and Ag⁺ translational modes in the far-IR region. For Na⁺ these modes occur at ca. 200–210 and 104–111 cm⁻¹. They have been described as correlated cation modes originating from E and A type local Na⁺ vibrations at C₃ six-ring sites, respectively.³⁹ At low silver concentrations, absorptions due to silver ion translational motions are very weak and are generally not resolved as separate bands, although they produce a shift in the peak position of the low frequency Na⁺ mode. In nearly completely exchanged sodalite, a characteristic Ag⁺ mode appears at 91–98 cm⁻¹. Full exchange is evident by the absence of the otherwise intense Na⁺ band at ca. 200–210 cm⁻¹. The greater mass of silver is a major factor contributing to the shift to lower frequency, with respect to Na⁺.

The cation and anion vibrations are coupled to various extents, depending on the interaction between the vibrating moieties. Thus the replacement of sodium by silver not only leads to the appearance of new far-IR absorptions associated with the cations but also produces changes in the anion translational modes of

(47) Stein, A. *M. Sc. Thesis* 1988, University of Toronto.

(48) Baker, M. D.; Godber, J.; Ozin, G. A. *J. Phys. Chem.* 1985, 89, 305, 2299.

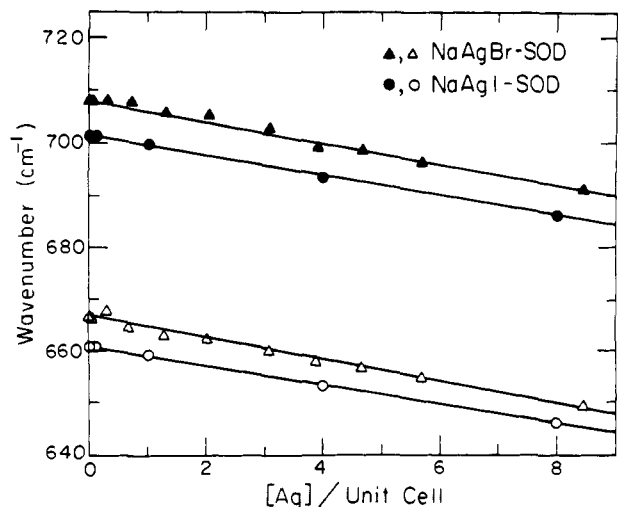


Figure 6. The dependence of the two T-O stretching frequencies in mixed sodium, silver halosodalites with various degrees of silver exchange.

Table IV. Frequencies of IR Framework Bands of Sodalites (cm⁻¹)

sodalite type	$\nu_{as}(T-O)^a$	$\nu_s(T-O)$	$\delta(O-T-O)$	$\delta(T-O-T)$
NaCl-SOD	981	738, 713, 671	469, 437	293
AgCl-SOD	982	719, 694, 654	461, 432	287
NaBr-SOD	986	733, 708, 667	465, 434	291
AgBr-SOD	987	715, 691, 650	459, 426	289
NaI-SOD	997	728, 701, 661	462, 431	288
AgI-SOD	986	710, 686, 646	456, 424	284

^a Broad, very strong absorptions. The peak position of this band varies slightly from sample to sample.

halosodalites. In the case of sodium chlorosodalite two correlation coupled chloride modes are found at ca. 174 (a shoulder) and 97 cm⁻¹, see Figure 5. Upon complete exchange with silver the absorption peaks shift to 185 and 138 cm⁻¹, displaying a smaller correlation splitting than in the starting sodalite. This indicates a reduced interaction between the anions in adjacent cages (mediated by the cations). Support for this idea is given by a monotonic shift to higher energy of the lower Cl⁻ translatory mode as the Ag⁺ concentration is increased. The anion modes of NaCl-SOD, NaBr-SOD, and NaI-SOD occurred at progressively lower frequencies as the anion mass increased. In contrast, the cation translational frequencies remained practically unperturbed upon variation of the anion. Upon exchange of NaBr-SOD and NaI-SOD with silver only one anion mode was observed in either case, in the range from 200–50 cm⁻¹, see Figure 5. The cation and anion translational modes have been studied systematically for different ions in sodalites and other zeolites.^{39,49}

Zeolite framework absorptions in the mid-infrared region have been studied in much detail.⁵⁰ Absorptions of sodalites and other framework silicates in the range 1300–400 cm⁻¹ fall into well-defined "fingerprint" regions. They originate from vibrations of TO₄ (T = Si or Al) tetrahedra in the framework (lattice vibrations), from vibrations within these TO₄ units (librational or translational modes) and combination vibrations.³⁹

Table IV lists the bands related to framework vibrations in the 1000–200-cm⁻¹ region for sodalites with various anion and cation content. The intense $\nu_{as}(T-O)$ asymmetric stretching modes of SiO₄ and AlO₄⁻ groups are typical of aluminosilicates in general. These vibrations tend to be insensitive to variations in the framework structure and the presence of extraframework guests. By contrast, the bands termed $\nu_s(T-O)$ and $\delta(O-T-O)$ are characteristic fingerprints of the sodalite structure. Their frequencies are sensitive to changes in the framework with changing extraframework ions and shift to lower energy after exchange of

silver for sodium. Cation vibrations involve direct interaction with neighboring framework oxygens. The ensuing local lattice distortion is the cause for the sensitivity of the framework vibrations to the cation type. For the symmetric Si or Al to O stretching modes of halosodalites, this shift is nearly linear with silver loading, as shown in Figure 6. A downward shift is observed by increasing not only the mass of the cation (Ag⁺ versus Na⁺) but also that of the anion (I⁻ versus Br⁻). With the help of calibration curves like these, mid-IR spectroscopy becomes a very fast quality control tool not only to verify the framework integrity of a sodalite sample but also to determine the silver concentration.

Solid State Nuclear Magnetic Resonance (NMR) Spectroscopy

While X-ray diffraction data provide details about the extended-range periodic structure of a crystalline lattice, solid state NMR informs us about shorter range interactions in the immediate environment of an NMR-active nucleus. The main features of solid state NMR spectra are determined by the local symmetry of the nucleus, rather than by the full point group symmetry of its site or the space group of the crystal.⁵¹ Another important difference is that while XRD methods can locate only the most stationary cations in zeolites, NMR measurements are most sensitive to mobile cations and cations in high symmetry sites.⁵² Solid state NMR has been a useful probe in the study of zeolites, providing information about their structure and dynamics. Good reviews on this subject include those by Engelhardt and Michel⁵³ and Klinowski.⁵⁴ In the following section we will present ²⁹Si, ²⁷Al, and ²³Na magic angle spinning (MAS) and double rotation (DOR)^{55–57} NMR data for class A sodalites.

The ²⁹Si MAS-NMR spectrum of an AgBr-SOD sample ($a_0 = 8.926$ (5) Å) displayed a single sharp resonance at -84.0 ppm versus TMS, consistent with the ordered array of silicon and aluminium and the sole existence of Si(OAl)₄ environments expected in these compounds with a Si:Al ratio of 1:1 (Loewenstein's rule). Exceptions have been found in sodalites with partially filled cavities and orientationally ordered tetrahedral anions (Na₃-(SiAlO₄)₆·MO₄, M = Cr, Mo, or W), where more than a single resonance was featured in the ²⁹Si spectrum.²⁹ Even though, according to the chemical analysis, up to 10% of the cages in this silver bromosodalite could have contained Ag₄OH³⁺ or Ag₃³⁺ aggregates (the ²⁹Si shift for AgOH-SOD is -81.3 ppm), the peak showed no asymmetry at higher frequency. These results suggest that the hydroxide- or anion-free cages do not form a separate phase but are distributed randomly throughout the lattice, although it may be difficult to detect a second phase at the 10% level, even in a physical mixture of AgBr-SOD and AgOH-SOD.

A bromosodalite with a low silver loading (NaAgBr-SOD, 0.68 Ag/uc, $a_0 = 8.941$ (2) Å) also showed only one sharp peak at -85.9 ppm, even though the sample contains several types of cages with different Na_{4-n}Ag_nBr³⁺ contents. This indicates that the electronic environment of the ²⁹Si nuclei is not strongly influenced by the silver guests. This may be a manifestation of very weak interaction of the silver ions with the tetrahedral framework atoms.

The chemical shift of NaBr-SOD compares to a literature value of -86.7 ppm.²⁹ The chemical shifts of the silver-exchanged bromosodalites follow the same trend as the shifts of sodalites studied by Weller and Wong,²⁹ i.e., they increase in magnitude for an increase in lattice constant. However, their magnitudes are slightly smaller compared to values listed by Weller and Wong

(51) van der Klink, J. J.; Veeman, W. S.; Schmid, H. *J. Phys. Chem.* **1991**, *95*, 1508–1511.

(52) Welsh, L. B.; Lambert, S. L. In *Characterization and Catalyst Development*; Bradley, S. A., Gattuso, M. J., Bertolacini, R. J., Eds.; ACS Symposium Series 411; American Chemical Society: Washington, DC 1989; pp 262–272.

(53) Engelhardt, G.; Michel, D. *High Resolution Solid-State NMR of Silicates and Zeolites*; John Wiley & Sons: 1987.

(54) Klinowski, J. *Prog. Nucl. Magn. Reson. Spectrosc.* **1984**, *16*, 237–209.

(55) Samoson, A.; Lippmaa, E.; Pines, A. *Mol. Phys.* **1988**, *65*, 1013–1018.

(56) Chmelka, B. F.; Mueller, K. T.; Pines, A.; Stebbins, J.; Wu, Y.; Zwaniger, J. W. *Nature* **1989**, *339*, 42.

(57) Chmelka, B. F.; Pines, A. *Science* **1989**, *246*, 71–77.

(49) Baker, M. D.; Ozin, G. A.; Godber, J. *Catal. Rev.-Sci. Eng.* **1985**, *27*, 591.

(50) Flanigen, E. M. In *Zeolite Chemistry and Catalysis*; Rabo, J. A., Ed.; ACS Monograph 171 American Chemical Society: Washington, DC, 1976; p 80.

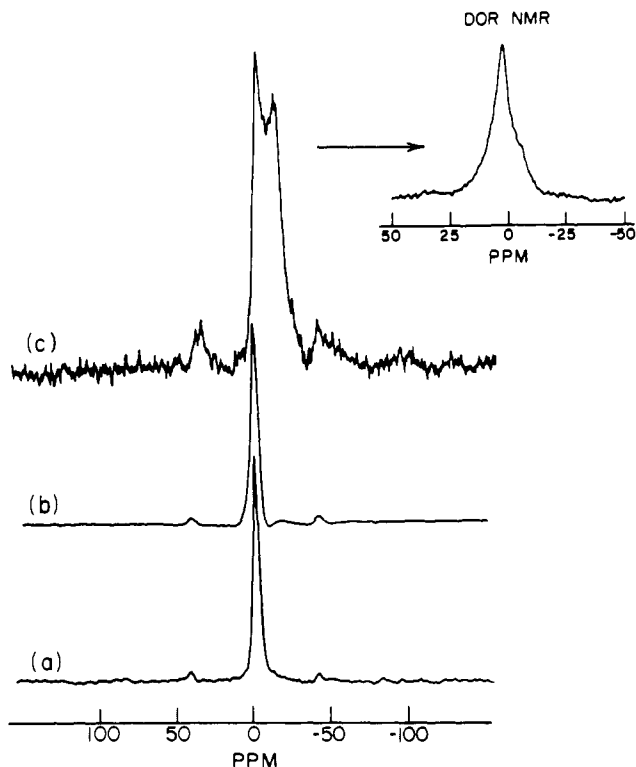


Figure 7. ^{23}Na MAS-NMR spectra at 7 Tesla of (a) NaCl-SOD, (b) NaBr-SOD, and (c) NaI-SOD. The inset shows the corresponding ^{23}Na DOR-NMR spectrum at 11.7 T for NaI-SOD.

for the corresponding lattice constants.

As ^{29}Si NMR could not distinguish between different cage contents, ^{27}Al was used as another probe. Because of quadrupolar broadening of ^{27}Al resonances in MAS-NMR, double rotation spectra were obtained for this nucleus instead. The ^{27}Al DOR-NMR spectra of partially silver-exchanged halosodalites showed only single sharp resonances: NaAgCl-SOD (4 Ag/uc, $a_0 = 8.866$ (3) Å) +62.2 ppm versus a dilute solution of $\text{Al}(\text{NO}_3)_3$; NaAgBr-SOD (5.66 Ag/uc, $a_0 = 8.925$ (3) Å) +62.2 ppm; NaAgI-SOD (4 Ag/uc, $a_0 = 8.984$ (3) Å) +59.3 ppm. Like the silicon atoms, the aluminum atoms experienced only one (average) environment, which may be partially dependent on the unit cell size and partially on the nature of the anion and cation. Details of this work will be presented in a separate publication.¹¹⁶

As discussed earlier, a question of great interest for silver sodalites is the distribution of silver throughout the lattice, or in other words, the distribution of clusters of the type $\text{Na}_n\text{Ag}_{4-n}\text{X}^{3+}$, $n = 0-4$. It was anticipated that this issue could be addressed most directly by ^{109}Ag or ^{23}Na NMR. No resonance could be detected by ^{109}Ag MAS-NMR⁵⁸ because of the low inherent sensitivity, negative gyromagnetic ratios, and long spin-lattice relaxation times of ^{109}Ag and ^{107}Ag ($I = 1/2$ for both isotopes).⁵⁹ However, it was found that for sodalites strong ^{23}Na signals could be observed readily both by MAS- and DOR-NMR spectroscopy.

^{23}Na MAS-NMR spectra were obtained for partially silver-exchanged and pure sodium halosodalites (chloride, bromide, and iodide). The spectra for the pure sodium halide forms appear in Figure 7. In the case of NaCl-SOD and NaBr-SOD only a single relatively narrow resonance is observed. DOR did not increase the resolution of these spectra, implying that the quadrupolar interactions of the sodium site are rather small. The NaI-SOD sample on the other hand displays a broad powder pattern. A DOR spectrum of NaI-SOD in 11.7 T magnetic field showed only a single narrow peak, confirming that the line shape of the resonance observed by MAS was largely due to quadrupolar effects.

Table V. ^{23}Na MAS- and DOR-NMR Resonances of Sodium, Silver Halosodalites^a

sample	Na/uc	Ag/uc	MAS shift (ppm)	DOR shift (ppm)
NaCl-SOD	8	0	-0.8 (-0.9)	
NaAgCl-SOD	7.9	0.1	-1.0	
NaAgCl-SOD	7	1	-1.1	
NaAgCl-SOD	4	4	-1.3	3.3
NaBr-SOD	8	0	-1.3 (-0.8)	
NaAgBr-SOD	7.7	0.05	-1.5	
NaAgBr-SOD	7.6	0.28	-1.5	
NaAgBr-SOD	7.2	0.68	-1.4	7.2, -1.8
NaAgBr-SOD	6.6	1.3	-1.7	
NaAgBr-SOD	6.1	2.0	-1.5	7.0, -1.9
NaAgBr-SOD	5.3	2.4	-1.7	
NaAgBr-SOD	4.6	3.1	-1.9	
NaAgBr-SOD	4.0	3.9	-3.3, -9.7	5.7, -1.9
NaAgBr-SOD	3.4	4.7	-3.4, -11.0	
NaAgBr-SOD	2.8	5.7	-3.1, -11.7	5.7, -1.9
NaI-SOD	8	0	-5.9, -10.1, -12.1 (-4.1, -15.5)	3.2
NaAgI-SOD	7.9	0.1	-6.7, -11.4	
NaAgI-SOD	7	1	-6.8, -11.1	3.4, -3.4 ^b
NaAgI-SOD	4	4	-12.2, -13.6	0.7, -3.6
NaCl			(0.0)	
NaBr			(-1.52)	
NaI			(-10.1)	

^a Notes: MAS shifts are given in ppm versus solid NaCl. They are not corrected for quadrupolar effects. Values in parentheses are from a second measurement on another spectrometer. DOR shifts are given in ppm versus a 1 M NaCl aqueous solution. Subtract ca. 7.9 ppm to compare with the MAS values. Silver and sodium concentrations of the bromide samples are from the chemical analysis and therefore do not necessarily add up to 8 M/uc. ^b Shoulder.

The larger quadrupole broadening observed for sodium in iodide-containing cages can be traced to the electronegativity difference between the iodide on one side of the Na^+ and the framework oxygens on the other. These values are $(\Delta(\chi_{\text{O}} - \chi_{\text{X}}) = 0.28, 0.48, 0.78$ for $\text{X} = \text{Cl}, \text{Br},$ and I , respectively (where χ is the Pauling electronegativity), and indicate higher charge asymmetry and consequently a larger electric field gradient for the Na^+ as the atomic number of the halide increases.

The chemical shift for sodium ranges approximately from 62.2 ppm versus an aqueous NaCl solution for Na^+ in tetrahydrofuran⁶⁰ to -20.4 ppm for solid NaClO_4 .⁶¹ In this study solid NaCl was used as a chemical shift reference for MAS, which has a shift of 7.9 ppm versus a 1 M NaCl aqueous solution.⁶¹ In the sodalites the ^{23}Na shifts were found to range from -0.9 ppm versus solid NaCl (+7.0 ppm versus 1 M NaCl) for NaCl-SOD to -14.0 ppm (-6.1 ppm versus 1 M NaCl) for NaOH-SOD. Even though the sodium ion near a sodalite six-ring is not unlike Na^+ in 18-crown-6 ether, the latter is shifted to much more negative values (18-crown-6, Na^+ : in nitromethane, -16.3 ppm; in acetonitrile, -14.9 ppm; in propylene carbonate, -16.2 ppm; in acetone, -15.8 ppm; in pyridine, -12.4 ppm versus 0.1 M NaCl in water).⁶² In a sodalite cage, the halides deshield Na^+ relative to the crown ethers in different solvents where no electronegative anion is coordinated to the Na^+ . The chemical shifts in the sodium sodalites follow the order of electronegativities: $\text{I} < \text{Br} \leq \text{Cl}$ (Table V). This is analogous to the bulk salts, for which the shifts versus 1 M NaCl aqueous solution are NaCl, 7.9; NaBr, 6.0; NaI, -2.7 ppm⁶¹ (see also Table V). The greatest shielding of sodium ions occurs in the presence of the least electronegative anion (iodide). The decreased electronegativity of I^- relative to Cl^- permits an overall greater electron density and increased shielding of Na^+ . Tabeta and Saito⁶¹ invoked a heavy atom effect (spin-polarization by the heavy iodide ion) to explain the considerable upfield shift for NaI compared to NaBr and NaCl. They also suggested that an increase in the Na-X distance leads to greater shielding, i.e., a more

(58) Plischke, J.; Benesi, A.; Vannice, A.; Ozin, G. A.; Stein, A., unpublished results.

(59) Henrichs, P. M. *NMR of Newly Accessible Nuclei* 1983, 2, 319-336.

(60) Ceraso, J. M.; Dye, J. L. *J. Chem. Phys.* 1974, 61, 1585-1587.

(61) Tabeta, R.; Saito, H. *Chem. Lett. (Jpn.)* 1984, 293-296.

(62) Graves, H. P.; Detellier, C. *J. Am. Chem. Soc.* 1988, 110, 6019-6024.

negative shift, because a higher electron density is created at the Na atom. This trend coincides with the halosodalites (Na-Cl, 2.704 Å, Na-Br, 2.888 Å, Na-I, 3.089 Å), although in this situation the changing Na-O distance will play a role. An additional contribution to the shielding of Na⁺ may arise from the flexing of the framework as the unit cell size increases. As the Si-O-Al angle α becomes larger, the charge density from the sodalite cage lattice six-ring oxygens to Na⁺(3s) decreases as that to Si^{IV} and Al^{III} increases. Further NMR experiments at two magnetic field strengths indicated, however, a subtle interplay between chemical shifts and quadrupolar effects that influence the position of the Na⁺ resonance.¹¹⁶

Partially exchanging sodium by silver leads to both changes in intensity (lower sodium concentration) and small chemical shifts to lower frequency (more negative ppm). Table V lists the ²³Na MAS-NMR chemical shifts measured for the NaAgX-SOD (X = Cl, Br, I) samples. These values are uncorrected, that is, they have been determined by peak picking rather than from a full line shape analysis. Therefore, for MAS spectra, the following discussion can only be considered qualitative. In the bromosodalite series, the shift remains relatively constant up to ca. 3 Ag/uc. At 4 Ag/uc, when half the cages are filled, on the average, a sudden jump occurs to lower frequency. At higher silver loadings (or lower sodium loadings) the shift remains fairly constant again. The greater shielding at high silver loadings may be associated with greater electron density on the sodium as it becomes less strongly associated with the central halide (increasing Na-Br distance). No obvious correlation exists between the ²³Na NMR peak positions and the unit cell sizes in this series. (In oxalatosodalites the ²³Na NMR shift was linearly correlated with the unit cell sizes.⁶³)

At low sodium concentrations a second resonance becomes apparent at lower frequency, first as a shoulder, and at even lower sodium concentrations as a resolved peak. This band was also observed by DOR-NMR and is therefore not due to quadrupolar line shifting or broadening effects. In DOR the low frequency peak shifts by ca. -1.6 ppm from the bromide series to the iodide series. The peak remains relatively constant in position with silver loading, even though the high frequency resonance moves abruptly at a minimum silver loading of ca. 4 Ag/uc, just as was observed by MAS-NMR. This is an indication that the sodium ions responsible for the low frequency peak do not experience a significantly different electronic environment as silver is exchanged into the halosodalite. According to MAS data, the position of the low frequency band is in the region of the sodium resonance in NaOH-SOD (-13.8 to -14.0 ppm versus solid NaCl) and Na-[]-SOD (-12.6 to -12.8 ppm versus solid NaCl). It is therefore assigned to a low percentage of hydroxide-containing or anion-free defect cages.^{64,65} A small difference in chemical shift may be due to the presence of bromide in adjacent cages. The fact that this resonance becomes more prominent at higher silver loadings but does not shift indicates that silver exchanges preferentially into halide-containing cages.^{65,116} Janssen et al.⁶⁶ also detected two types of cages in what they call "hydrated Cl-sodalites", although they did not recognize the fact that the second site was due to hydroxide-containing or anion-free cages. Their data confirm our conclusions: the Na nuclei associated with defect cages exhibited fast spin relaxation (ca. 10⁵ s⁻¹), brought about by the mobility of water molecules in these cages; spins in Cl cages relaxed more slowly (<10⁵ s⁻¹).

Only one resonance related to sodium in a halide cage is present, regardless of the silver concentration. Even though it appears that at a certain threshold silver loading this resonance is affected by

Table VI. Ion Charges Calculated by EHMO Theory

cluster	charge iterations			no charge iterations		
	Cl	Na	Ag	Cl	Na	Ag
Na ₄ Cl ³⁺	0.40	0.65		-0.20	0.80	
Na ₃ AgCl ³⁺	0.49	0.65	0.55	0.22	0.82	0.32
Na ₂ Ag ₂ Cl ³⁺	0.58	0.65	0.56	0.58	0.84	0.37
NaAg ₃ Cl ³⁺	0.66	0.64	0.57	0.89	0.87	0.41

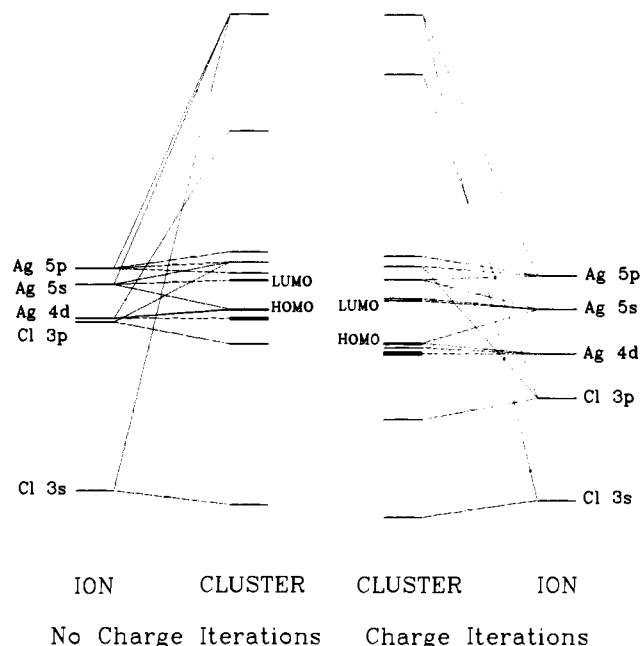


Figure 8. Molecular orbital diagram of Ag₄Cl³⁺ and the corresponding silver and chloride ion levels, calculated with and without charge iterations.

the silver content, ²³Na NMR could therefore not be used to determine the distribution of cations. The apparent insensitivity of the sodium signal to different cluster compositions Na_nAg_{4-n}X³⁺, $n = 0-4$, was corroborated by extended Hückel molecular orbital calculations (see below) which indicated that the major change in electron density is taken up by the anion as n changes, Table VI.

Extended Hückel Molecular Orbital (EHMO) Calculations

EHMO calculations were carried out on a number of silver halide clusters as well as on an individual sodalite cage with zero to four Ag₄Cl⁺ clusters, in order to investigate the nature of the bonding orbitals, those orbitals which are expected to be involved in the electronic transitions, the overlap of cluster orbitals with each other and with framework orbitals, and to examine the possibility of electronic band formation.

The atomic coordinates were normally fixed at the values obtained from X-ray structural refinement of silver halosodalites. No further geometry optimization was carried out to minimize total energies.

Trends in electronic structure with composition were studied without including the sodalite framework, because of the limited number of atoms that can be used in the ICONCL program. All clusters of the type M₄X³⁺ were found to be unstable (positive sums of stabilization energy and core-core repulsion energy). Addition of the framework stabilized the clusters. Diatomic AgX molecules (X = Cl, Br, I) were stable by themselves. The large positive charge on the other clusters leads to large repulsions which must be compensated for by the aluminosilicate framework. These conclusions coincide with experimental observations for silver halide clusters: while AgX is stable in the gas phase (as the monomer⁶⁷⁻⁷² or the trimer⁷³), Ag₄X is found only when stabilized

(63) Ozin, G. A.; Stein, A.; Stucky, G. D.; Godber, J. P. In *Inclusion Phenomena and Molecular Recognition*; Atwood, J., Ed.; Plenum Press: New York, 1990; pp 379-393.

(64) Stein, A.; Ozin, G. A. Sodalite, An Old Material for Advanced Uses. In *Advances in the Synthesis and Reactivity of Solids*; Mallouk, T. E., Ed.; 1991; Vol. 3, in press.

(65) Stein, A. Ph.D. Thesis University of Toronto, Canada, 1991.

(66) Janssen, R.; Breuer, R. E. H.; de Boer, E.; Geismar, G. *Zeolites* **1989**, 9, 59-67.

(67) Patel, M. M.; Nene, S. G. *Indian J. Pure Appl. Phys.* **1982**, 20, 247-248.

Table VII. Percentage Overlap between Atomic Orbitals within a Ag_4Cl Cluster, between Next Neighbors in Adjacent Clusters and with Framework Atomic Orbitals

orbital	(a) same cluster			(b) next cluster			(c) framework					
	Ag5s	Ag5p	Ag4d	Ag5s	Ag5p	Ag4d	Al3s	Al3p	Si3s	Si3p	O2s	O2p
Cl 3s	19	22	6					1				
Cl 3p	15	11	7					2				
Ag 5s	6	12	3	2	6	1	19	23	14	16	11	10
Ag 5p	12	19	4	6	13	2	30	25	26	22	25	14
Ag 4d	3	4	1	1	2	3	4	6	4	5	7	6

by a sodalite framework (this study) or in solution.^{41,42,74}

Figure 8 shows an MO diagram of $\text{Ag}_4\text{Cl}^{3+}$ with and without charge iterations. Charge iterations resulted in stabilization of all atomic orbitals and thus stabilization of most filled and some unfilled molecular orbitals. The greatest shift to lower energy occurred for Cl 3p AOs. Charge iterations resulted in a small redistribution of positive charge, placing a slightly higher positive charge on the more electropositive silver atoms. In all cases the positive charge was distributed evenly across all silver atoms, but a large positive charge remained on the Cl⁻ atom. The LUMO orbitals always possessed Ag 5s and Ag 5p characteristics, while the HOMO orbitals were mixtures of mainly X *np* (X = Cl 3, Br 4, I 5) and Ag 4d orbitals with some Ag 5s and Ag 5p character. The latter can therefore be considered as the Ag-X bonding orbitals. The large overlap of Ag 4d orbitals with halogen p orbitals and the resulting significant quantum mechanical mixing of p and d states in the valence band has been noted for the bulk silver halides.^{73,75} The calculated HOMO-LUMO gap was smaller for X = Br, I than X = Cl, although care must be taken when comparing results for different halides because of the neglect of spin-orbit effects in these calculations.

The effect of the number of clusters, *n*, on the frontier orbital levels was studied for $[\text{Ag}_4\text{Cl}^{3+}]_n$ cluster aggregates. The clusters were arranged in a space-filling cubic arrangement, as they would be in a body centered cube of nine sodalite cages (cf. Figure 2). Even though the absolute energies obtained with and without charge iterations differed greatly, the general trend observed was the same. The gap was reduced for larger *n*. The greatest change occurred for the first four clusters. When *n* = 9, the frontier orbital energies had nearly leveled out.

Figure 9 shows density-of-states diagrams (number of molecular orbitals in an energy interval of 0.25 eV) for $[\text{Ag}_4\text{Cl}^{3+}]$ and $[\text{Ag}_4\text{Cl}^{3+}]_{10}$. The framework was neglected in these calculations, but similar results were obtained when the framework was included for small *n*. One can see that while splitting of levels occurs and the density of levels increases at larger *n*, the overall pattern remains and levels still appear to be discrete. The following question arises: are valence and conduction bands formed upon the addition of more clusters? The overlap matrix, Table VII columns a and b, shows the orbital overlap (elements of the overlap matrix) between Cl, Ag, and Ag orbitals in the same cluster as well as the closest Ag's in an adjacent cluster. One can see that in spite of the relatively large Ag-Ag distances (4.14 Å (a) and 4.92 Å (b)) significant overlap still exists, even between adjacent clusters. As the interaction between atoms is proportional to the overlap integrals,⁷⁶ silver atoms are clearly interacting electronically, thus supporting the notion of bands. The large interaction radius of Ag atoms compared to, for example, other members of the noble metal family (e.g., Cu) has been discussed by Calzaferri

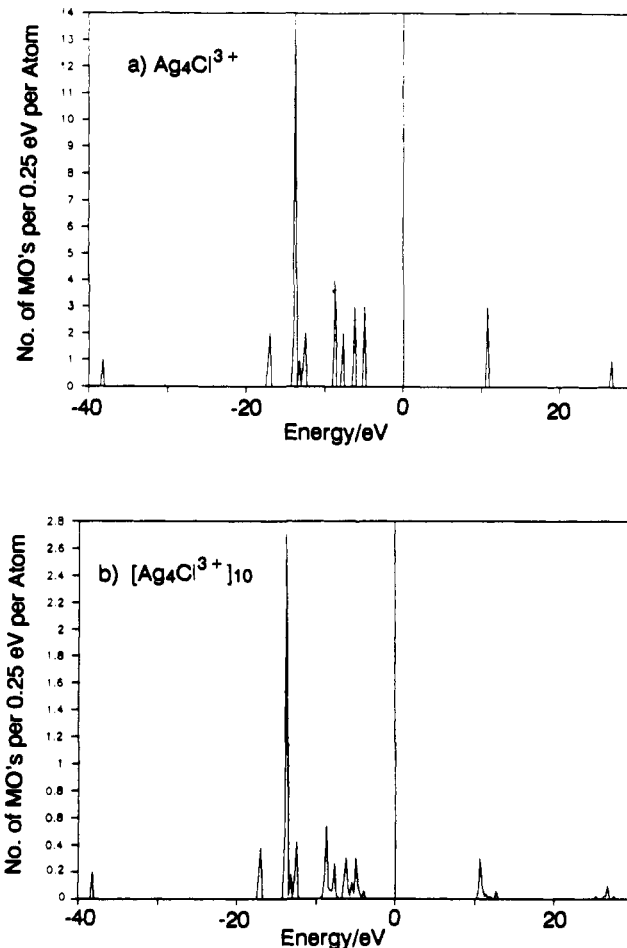


Figure 9. Density-of-states diagrams for (a) $\text{Ag}_4\text{Cl}^{3+}$ and (b) $[\text{Ag}_4\text{Cl}^{3+}]_{10}$. The graphs show the number of molecular orbitals per atom within 0.25 eV ranges.

and Forss,⁷⁶ who attributed some of the specific properties of silver zeolites to this behavior.

So far, we have treated these clusters as "gas phase species". However, in the sodalite cage they are part of a lattice which is composed of the additional atoms Si, Al, and O. A question one can justifiably ask is whether or not the framework atoms can really be treated as innocent bystanders, or whether they are involved in the interaction between clusters, or even within one cluster.

Figure 10 shows the density-of-states diagrams for an individual sodalite cage, a cage with two clusters (one at the center of a cage, one outside) and a cage with four clusters (one cluster at the center of the cage, three outside; this was the maximum number of clusters possible with the program). The structure of the cluster band is clearly visible, even within a sodalite cage (cf. Figure 9). The HOMO pertaining to the cluster is slightly destabilized by the presence of the cage. Mixing of framework and guest levels is also visible, especially in the LUMO region, where it leads to some orbital stabilization. At high cluster loadings, band broadening becomes more pronounced, and the orbital mixing is more extensive. In a similar calculation for a single cage,⁷⁶ Calzaferri and Forss did not see any band formation for cage

(68) Nair, K. P. R.; Hoefft, J. *Chem. Phys. Lett.* **1983**, *102*, 438-439.

(69) Nair, K. P. R.; Hoefft, J. *Phys. Rev. A* **1984**, *29*, 1889-1894.

(70) Nair, K. P. R.; Hoefft, J. *J. Phys. B: At. Mol. Phys.* **1984**, *17*, 735-738.

(71) Hoefft, J.; Nair, K. P. R. *Chem. Phys. Lett.* **1986**, *129*, 538-540.

(72) Nair, K. P. R.; Hoefft, J. *Phys. Rev. A* **1987**, *35*, 668-672.

(73) Potts, A. W.; Lyus, M. L. *J. Electron Spectrosc. Relat. Phenom.* **1978**, *13*, 305-315.

(74) Nilsson, K.; Persson, I. *Acta Chem. Scand.* **1987**, *A41*, 139-145.

(75) Bassani, F.; Knox, R. S.; Beall Fowler, W. *Phys. Rev. A* **1965**, *137*, 1217-1225.

(76) Calzaferri, G.; Forss, L. *Helv. Chim. Acta* **1987**, *70*, 465-479.

(77) Rossetti, R.; Hull, R.; Gibson, J. M.; Brus, L. E. *J. Chem. Phys.* **1985**, *83*, 1406-1410.

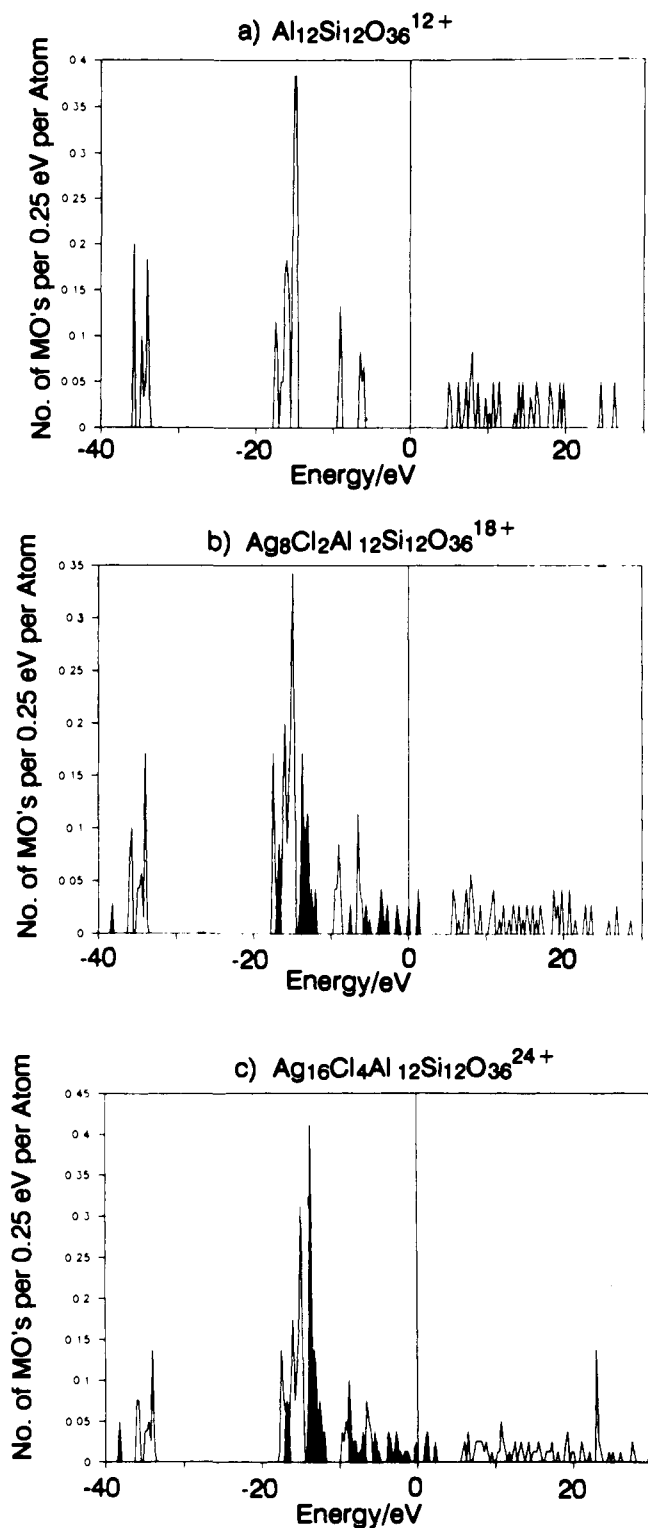


Figure 10. Density-of-states diagrams for an individual cluster-free sodalite cage, $\text{Al}_{12}\text{Si}_{12}\text{O}_{36}^{12+}$, a sodalite cage with two clusters (one inside, one outside), $\text{Ag}_8\text{Cl}_2\text{Al}_{12}\text{Si}_{12}\text{O}_{36}^{18+}$, and a sodalite cage with four clusters (one inside, three outside), $\text{Ag}_{16}\text{Cl}_4\text{Al}_{12}\text{Si}_{12}\text{O}_{36}^{24+}$. Regions pertaining mainly to the cluster orbitals are shown in dark.

atoms yet. But it is known that, for example, in ZnS and CdS, a crystallite must contain ca. 10 000 atoms before the bandgap characteristics for the bulk material are fully developed.⁷⁷ By analogy, a larger number of sodalite cages should likely lead to band formation.

While the HOMO still has the Ag 4d, Cl 3p, and Ag 5s characteristics, the LUMO now belongs to the framework Si 3s and Si 3p orbitals with some Ag 5s mixed in. An electronic transition between HOMO and LUMO would therefore involve

metal to framework charge transfer. As the LUMO level lies lower than the respective Ag 5s, Ag 5p mixture in $\text{Ag}_4\text{Cl}^{3+}$ clusters in the absence of the sodalite cage, the energy gap is now narrower. It is also significantly narrower than that of a sodalite cage containing $\text{Na}_4\text{Cl}^{3+}$ clusters (see Figure 13) or that of the hypothetical sodalite cage lacking any cluster atoms. In the latter case the lowest energy transition occurs from O 2p to Si 3s, Si 3p orbitals. This type of charge transfer transition is common in sodalites, zeolites, and other aluminosilicates or silicates.⁷⁸

The above calculations addressed pure silver halide clusters. Additional calculations were carried out on mixed Ag/Na halide clusters which are found in partially Ag-exchanged sodalites. For simplicity, only single clusters were modelled. Similar results are expected for larger cluster aggregates. The major difference in orbital characteristics compared to pure Ag clusters is the participation of Na 3s orbitals in the LUMO (together with Ag 5s and Ag 5p). The HOMO remains a mixture of Cl 3p, Ag 4d, and a little Ag 5s (in $\text{Na}_4\text{Cl}^{3+}$ it is composed of Cl 3p and a little Na 3s). While the HOMO-LUMO gap is large in the absence of silver, it shifts red as soon as at least one Ag atom is included in the cluster. The red shift continues with an increasing silver content ($[\text{Na}_4\text{Cl}]_9 \rightarrow [\text{Na}_4\text{Cl}]_8[\text{AgNa}_3\text{Cl}] \rightarrow [\text{Na}_4\text{Cl}]_7[\text{Ag}_4\text{Cl}] \rightarrow [\text{Ag}_4\text{Cl}]_9$), but the incremental change is smaller than after addition of the first silver. When the first silver atom is added, the frontier orbitals take on new characteristics (i.e., those pertaining to Ag^+ rather than Na^+). With addition of more Ag^+ , communication between the levels leads to stabilization of the LUMO and destabilization of the HOMO but does not change the identity of these levels drastically. Thus the change in the energy gap is smaller. This behavior coincides with the observed trend in UV-visible reflectance spectra of sodium, silver halosodalites (see below).

Optical Spectroscopy

Figure 11 shows UV-visible reflectance spectra for sodalites containing each of the three difference halides Cl, Br, and I, at silver loadings of 0, 0.1, and 8 Ag^+ per unit cell. In all cases the positions of the absorption bands show a halide dependence, the most dramatic difference occurring for the iodosalites.

The spectra of the sodium chloro- and bromosodalites consist of an absorption at ca. 205 nm with a shoulder around 240–250 nm. The iodide spectrum is more complex, with bands at 225–250 and 290 nm and a shoulder near 255 nm.

When a small amount of silver ions is present (0.1 Ag^+ /uc), new features appear, progressively red-shifted for the bigger anions in larger unit cells in the series Cl, Br, and I. The transitions are similar to the gas phase values of 230 and 320 nm for the AgBr monomer.⁷⁹ The effect of changing the silver concentration on the optical spectra is shown for the bromide series in Figure 12. At higher silver loadings the intensity of these components increases, but in the case of Cl and Br no significant shift in the absorption energy is observed. Again, the iodide sample behaves differently, showing a red-shift at increased silver loading for the major components.

After complete silver exchange the spectral features appear simpler again. A sharp absorption between 245 and 250 nm is superimposed on a broader feature peaking in the same region. Another peak or shoulder is present between 280 and 300 nm. The absorption bands are broadest for iodide. By comparison, the parity forbidden (Laporte forbidden) transitions generally described as $\text{Ag}(4d^9 5s)^1D \leftarrow \text{Ag}(4d^{10})^1S$ for the intraionic excitation of Ag^+ occur at the following wavelengths in alkali halides and more open zeolites: Ag^+ in NaCl, 245; NaBr, 275; KBr, 310; Ag^+ in $\text{Ag}_{0.1}\text{A}$, 207, 224, 240; in Ag_{11}A , 223, 233, 243 nm.⁸⁰

(78) Garbowski, E. D.; Mirodatos, C. *J. Phys. Chem.* **1982**, *86*, 97.

(79) Huber, K. P.; Herzberg, G. *Molecular Spectra and Molecular Structure, IV. Constants of Diatomic Molecules*; Van Nostrand Reinhold: New York, 1979.

(80) Texter, J.; Gonsiowski, T.; Kellerman, R. *Phys. Rev. B* **1981**, *23*, 4407.

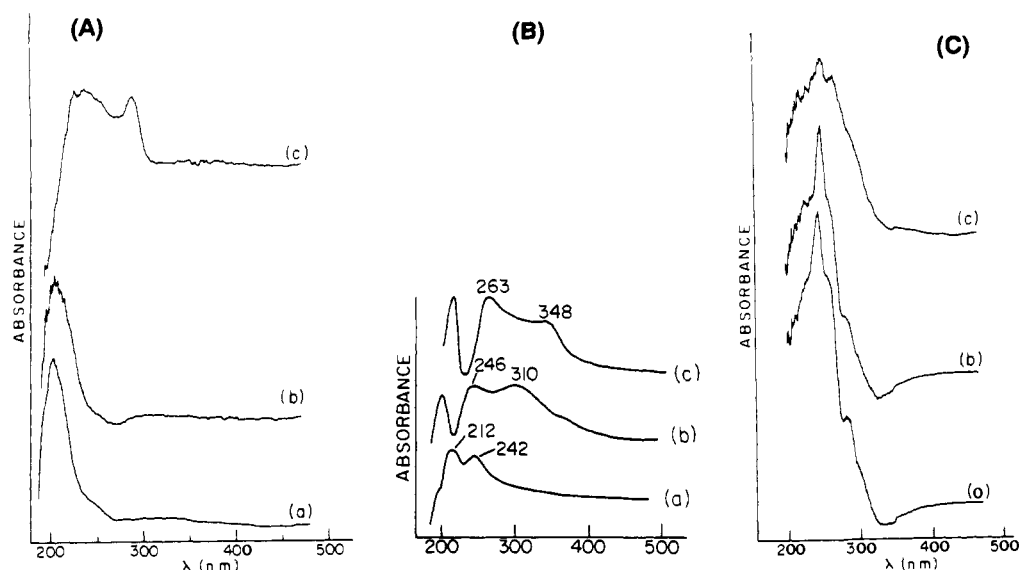


Figure 11. UV-visible reflectance spectra of sodium, silver halosodalites: (Aa) NaCl-SOD, (Ab) NaBr-SOD, (Ac) NaI-SOD, (Ba) NaAgCl-SOD, 0.1 Ag/uc, (Bb) NaAgBr-SOD, 0.1 Ag/uc, (Bc) NaAgI-SOD, 0.1 Ag/uc, (Ca) AgCl-SOD, (Cb) AgBr-SOD, and (Cc) AgI-SOD.

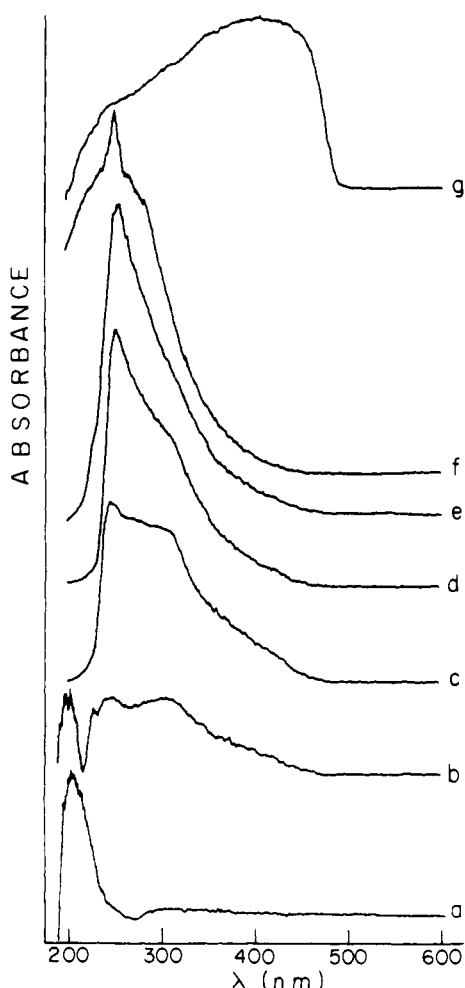


Figure 12. UV-visible reflectance spectra of sodium, silver bromosodalites with varying silver concentrations: Ag/uc (a) 0, (b) 0.05, (c) 0.28, (d) 2.0, (e) 3.1, (f) 8.0, and (g) bulk AgBr.

In many other host matrices containing quantum size particles, an increase in the loading of the semiconductor material results in a red-shift as the particle size increases.^{81,82} Inside the sodalites the I-VII cluster nuclearity is limited to five, and no significant

absorption band shifts occur at higher loadings for the Cl⁻, Br⁻ series, in contrast to the I⁻ series. The difference for the I⁻ series appears to originate in the more pronounced sensitivity of the sodalite unit cell dimensions (inter-β-cage distances and coupling) to Ag⁺ ion loading ($\Delta a_0 = 0.06 \text{ \AA}$), compared to the chloride and bromide series ($\Delta a_0 = 0.02 \text{ \AA}$). Significant overlap of atomic orbitals within a cluster as well as overlap of Ag 5p orbitals between adjacent clusters and through framework atoms allows electronic communication between cages and the content of cages.

The energy levels due to clusters with 0, 1, 2, 3, and 4 silver ions are likely to overlap and merge into common bands of the types O 2p, Ag 4d, {X *np*, Ag 5s, 5p, 4d}, and {[Na 3s, Ag 5s] Si 3s, 3p}. [Braces around orbitals imply orbital mixing, brackets imply the presence of either one or more orbitals included in the list.] An averaged energy level diagram is expected, which dampens any spectral changes related to Ag⁺ loading. Even after complete silver exchange the absorption edge remains at higher energy than in bulk AgBr, an indication that microcrystalline AgBr is absent.

A study of the temperature dependence of the absorption spectra for silver halosodalites between 26 and 318 K indicated that the absorption intensities remained nearly constant with temperature, except for the broad absorption centered around 250 nm. This absorption is nearly absent at low temperatures, resulting in greater resolution of the remaining absorption bands. As the temperature increases this band becomes more intense and broadens. At the same time it undergoes a slight blue shift.

In order to assign the transitions involved in the above absorptions, it is helpful to consider the quasi energy band diagrams obtained by extended Hückel molecular orbital (EHMO) calculations, Figure 13. The calculations are based on a single sodalite cage with the composition $M_4XAl_{12}Si_{12}O_{36}^{15+}$. The number of atoms used is that number required to complete one cage, which does not coincide with one-half of a unit cell. As no terminal atoms (e.g., hydrogen) were included, the charge on the cage, excluding the M_4X cluster, is 12+. The Wolfsberg-Helmholz-Calzaferri weighting formula^{83,84} was used; no charge iterations were carried out. Closely spaced energy levels of the same orbital composition are represented as continuous bands, to simplify the diagram.

The framework atoms are involved in the optical transitions via the O 2p and Si 3s, 3p orbitals. According to the EHMO calculations, the Al 3s, 3p levels lie too high to take part in the transitions. In the absence of silver, the Cl 3p levels mix in with

(83) Ammeter, J. H.; Bürgi, H.-B.; Thibeault, J. C.; Hoffmann, R. *J. Am. Chem. Soc.* **1978**, *100*, 3686-3692.

(84) Calzaferri, G.; Forss, L.; Kamber, I. *J. Phys. Chem.* **1989**, *93*, 5366-5371.

(81) Brus, L. E. *Nouv. J. Chim.* **1987**, *11*, 123.

(82) Henglein, A. *Top. Curr. Chem.* **1988**, *143*, 113.

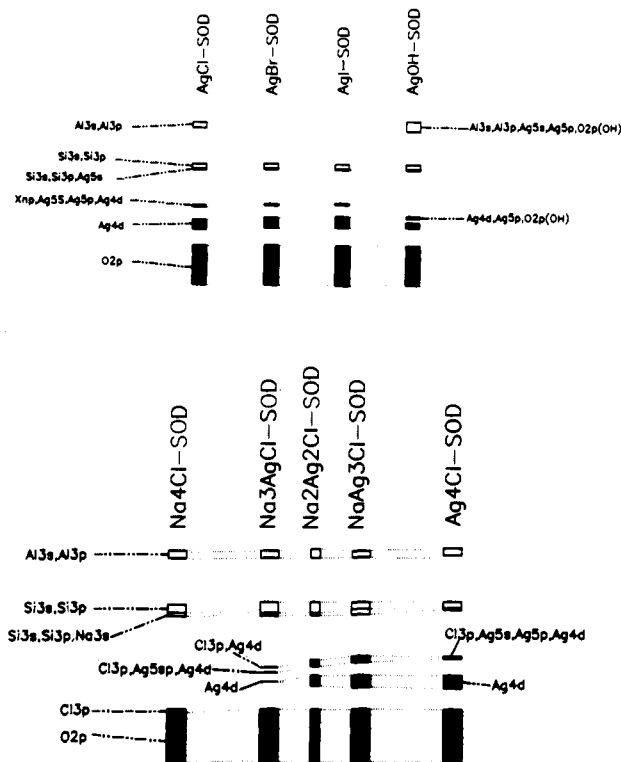


Figure 13. Sodalite band diagrams for one cluster of the type indicated, inside a single sodalite cage.

the more energetic O 2p levels, while Na 3s mixes with lower energy Si 3s, 3p levels. No mixed Na/Cl bonding orbitals are present. The bandgap is hardly affected, corresponding mainly to a Si ← O ligand-to-metal charge transfer (205-nm absorption). The shoulder found at lower energy may correspond to optical transitions within the cluster (Na ← Cl). The band broadening and greater spectral complexity for the iodide sample may be related to the increased spin-orbit coupling for this heavy halide.

When some sodium ions are replaced by silver ions, new levels appear within the sodalite framework bandgap. While cation s orbitals still mix with Si 3s, 3p, the halide p orbitals move above the O 2p in energy, mixing with silver orbitals instead. This mixing is an indication of Ag–X bonding. In addition to the framework charge transfer transition, the spectra in Figure 11 now show features corresponding to transitions from Ag 4d or halide p mixed with Ag 5s, 5p or 4d to mixed $\{[Na\ 3s, Ag\ 5s] Si\ 3s, 3p\}$ LUMO levels. The fact that the LUMO consists of both cluster and framework orbitals indicates that the aluminosilicate framework is involved in the electronic interactions between clusters and affects the optical and electronic properties of silver sodalites.

As the silver loading is increased, the Ag 4d band broadens, while the separate Cl 3p, Ag 5s, 5p, 4d bands merge into one sharper, destabilized band. For completely silver-exchanged samples, the optical absorptions can be assigned to $\{Si\ 3s, 3p\} \leftarrow \{Ag\ 4d\}$ (broader 245–250-nm absorption); $\{Si\ 3s, Si\ 3p, Ag\ 5s\} \leftarrow \{Ag\ 4d\}$ (sharp 245–250-nm absorption); $\{Si\ 3s, 3p, Ag\ 5s\} \leftarrow \{X\ np, Ag\ 5s, 5p, 4d\}$ (280–300 nm). The first two transitions do not involve halide orbitals, and the corresponding optical absorptions show little halide dependence. (The sharp absorption band is absent in Ag []-SOD samples whose cages contain water instead of a halide ion.²) The energy of the $\{Si\ 3s, 3p, Ag\ 5s\} \leftarrow \{X\ np, Ag\ 5s, 5p, 4d\}$ transition exhibits a slight dependence on the type of halide. The almost negligible narrowing of the calculated energy gaps for the series Cl, Br, and I is due mainly to a small destabilization of the HOMO on going down the halogen group. In a study of AgBr mixed silver halides, Marchetti and Burberry⁸⁵ also observed a decrease in the bandgap energy as the iodide content was increased, caused by an upward shift of the

Table VIII. Bandedges of AgX-SOD

sample	bandedge (eV)		
	overall	best	EHMO
AgCl-SOD	3.83 ± 0.05	3.78 ± 0.05 if	2.52
AgBr-SOD	3.85 ± 0.05	3.79 ± 0.08 if	2.45
AgI-SOD	3.75 ± 0.09	3.77 ± 0.14 ia	2.36
	3.08 ± 0.07	3.09 ± 0.06 ia	

valence band (also Berry⁸⁶). As the LUMO does not involve halide orbitals, it remains virtually unaffected by the halide (except for changes caused by different unit cell sizes). The framework charge transfer transition is still present underneath the more intense silver related absorptions.

The absorption edges of silver halides and other semiconductors have been fitted to standard equations,⁹³ to determine the allowedness of the interband transitions. Because the nuclearity of the Ag_nX^{3+} clusters is small, the lowest energy absorptions may be simply due to HOMO–LUMO transitions of a molecular nature. However, the observations that (1) silver ions from adjacent clusters can overlap directly as well as via framework atoms and (2) absorption band broadening occurs for greater connectivity between clusters² suggest that the formation of bands may be possible in silver halosodalites. Narrow bands may occur in insulators and metals when valence electrons have both localized and band-like characteristics. They can also occur in situations where interatomic distances are so large that the only mechanism for broadening is via an excited state of one or more atoms involved. This mechanism applies, for example, to transition metal halides in which cation–cation distances are very large,⁸⁷ i.e., systems not unlike the clusters under consideration. Assuming that band theory concepts and the k-selection rule are applicable (i.e., that a band description is valid), the absorption edges of AgCl-SOD, AgBr-SOD, and AgI-SOD above 300 nm were fitted according to ref 93. In all cases the fit for a da transition was worst, while df, ia, and if all showed straight line parts, the fits for the indirect transitions appearing to be best. Table VIII lists the fitted bandedges. The “overall” value is an average of the values for df, ia, and if; the “best” value is the energy with the least uncertainty in the intercept. (If phonons are involved in AgI-SOD, $\hbar\omega + \hbar\omega_c = 3.77$ eV, $\hbar\omega - \hbar\omega_c = 3.09$ eV. Therefore $\hbar\omega = E_g = 3.43 \pm 0.20$. This is not the case if AgI-SOD behaves like a heavily doped semiconductor, see below.) These values are significantly smaller than the optical bandgaps in sodium sodalites,⁸⁸ which show a strong halide dependence: NaCl-SOD, 6.1; NaBr-SOD, 5.9; NaI-SOD, 5.2 eV.

Except for the fact that AgI-SOD displayed a second component in the absorption tail, the gaps for the three silver halosodalites are not significantly different from each other. This is in qualitative agreement with the gap calculated by the EHMO method, which also varies only very slightly with the type of halide. The interband transitions appear to be indirect, i.e., the bottom of the conduction band is at a different *k*-value than the top of the valence band. The lowest energy interband transitions in bulk AgCl and AgBr (allowed⁸⁹) are also indirect.⁹⁰ β -AgI (wurtzite) is a direct gap ionic semiconductor.^{77,91,92} The allowedness of a transition is normally determined experimentally.⁹³ However, because of the similarity in the fits for ia and if, our data did not allow us to distinguish between allowed and forbidden processes. Energy band calculations in *k*-space are required to characterize

(86) Berry, C. R. *Photogr. Sci. Eng.* **1975**, *19*, 93–95.

(87) *Narrow Band Phenomena, Influence of Electrons with Both Band and Localized Character*; Fuggle, J. C., Sawatzky, G. A., Allen, J. W., Eds.; Plenum Press: New York, 1988.

(88) van Doorn, C. Z.; Schipper, D. J.; Bolwijn, P. T. *J. Electrochem. Soc.* **1972**, *119*, 85.

(89) Kawate, E.; Masumi, T. *J. Phys. Soc. Jpn.* **1988**, *57*, 1814–1819, 1820–1825, 1826–1833.

(90) Sturmer, D. M.; Marchetti, A. P. In *Imaging Processes and Materials*, 8th ed.; Sturge, J., Walworth, V., Shepp, A., Eds.; Van Nostrand Reinhold: New York, 1989; pp 71–109.

(91) Micic, O. I.; Meglic, M.; Lawless, D.; Sharma, D. K.; Serpone, N. *Langmuir* **1990**, *6*, 487–492.

(92) Vucemilovic, M. I.; Micic, O. I. *Radiat. Phys. Chem.* **1988**, *32*, 79–83.

(85) Marchetti, A. P.; Burberry, M. *Phys. Rev. B* **1988**, *37*, 10862–10866.

the interband transitions in silver halosodalites in more detail.

Photon absorption in indirect bandgap materials must involve a momentum-conserving process. In many cases (e.g., in AgBr)⁹⁴ phonon absorption or emission assists the electron in an indirect transition. In those cases one would expect the bandgap energy to be temperature dependent, due to increasing phonon absorption with increasing temperature. Yet in the case of the silver halosodalites the temperature dependence of the edge was found to be very small. This behavior points to either a "localized" cluster description or, if a band model is valid, to the possibility of alternate momentum-conserving processes, such as the scattering processes found in heavily doped indirect bandgap semiconductors.^{85,93} In such materials the absorption coefficient is similar to that for an indirect allowed transition, except that the Bose-Einstein population factor for phonons does not appear. Our data are unable to distinguish between this process and the *df*, *ia*, and *if* ones described above. The alternate processes conserving crystal momentum involve impurities or disorder, which destroy the *k* selection rule by destroying translational symmetry. The silver sodalites are known to contain hydroxide or [] cage impurities. They also contain framework defects (especially at the surface). In addition, samples with low silver loading show cation disorder.

Conclusions

This investigation showed that sodium, silver halosodalites may be used to fabricate an organized assembly ranging from "isolated molecules" to an expanded cluster lattice of a material that is normally a I-VII semiconductor, stabilized inside a sodalite host matrix. Control over the silver halide environment was possible by varying the anion and cation composition, which involved alteration of the unit cell size.

The unit cell sizes of class A sodalites depend on the silver concentration and on the type of halide. Short molecular-like Ag-X distances were observed at low silver concentration. At increased Ag⁺ concentrations up to complete silver exchange the product is better described as a sodalite lattice containing an "expanded silver halide". Both far-IR and XRD data showed sudden breaks at a silver loading corresponding to more than one Ag⁺ per sodalite cage, possibly indicating a percolation threshold. The UV-visible absorption edge was not highly dependent on silver concentration, consistent with the limitation of the cluster nuclearity to five. Absorption lines could be assigned to transitions involving both the guest clusters and the sodalite framework.

A key question is how much interaction exists between the sodalite host matrix and the guest species, whether they are so-called "isolated molecular species" or expanded cluster supralattices. In NaCl-SOD, Na⁺ and Cl⁻ are clearly part of the whole unit cell. For example, the sodium ions are closely associated with the six-ring oxygens. One can justifiably ask whether or not the Ag₄Cl clusters act as almost independent moieties, slightly perturbed by the framework or even as a collective (Ag₄Cl)_n sublattice. An interaction would apply to both directions: the effect of the host on the guest and the effect of the guest on the host. The presence and identity of the cations and anions inside the sodalite cages clearly affected the aluminosilicate framework, by causing it to flex and adapt its size to the ions. This effect was also apparent in the framework vibrations. The electronic effect was small. EHMO calculations indicated that electronic levels associated with framework atoms remained almost unaffected, except for some mixing of silver levels at the top of the O 2p and bottom of the Si 3s, 3p bands.

To examine the reverse effect, the perturbation of silver halide clusters by the aluminosilicate framework, one can compare the bond lengths between cations and anions or cations and framework oxygen atoms to the distances found in related compounds. The silver-halide distances were longest in fully silver-exchanged sodalites. Even then they were ca. 8% shorter than in the rock-salt (AgCl, AgBr) or zinc-blende (AgI) bulk materials. The Ag-I separation was nearly identical to that found in other silver iodide

Table IX.^{a,b}

product	xAl(OH) ₃	ySiO ₂	zNaOH	vH ₂ O	wNa _{1,2} X	salt
NaCl-SOD	1	2	6	80	5	NaCl
NaBr-SOD	1	1	12.5	144	7.5	NaBr
NaI-SOD	1	2	6	80	5	NaI

^aNote: all values are given in moles, relative to 1 mole Al(OH)₃.
^bList of reagents for sodalite synthesis and silver exchange: Al(OH)₃, Fisher, 99.8%; SiO₂, Ludox HS-30, Ludox HS-40 (Dupont), Luddy (40%, Alchem) (colloidal aqueous silica sources); NaOH, Mallinckrodt, 98.7%; H₂O, deionized; NaCl, BDH, 99.0%; NaBr, Mallinckrodt, 99.0%; NaI, BDH, 99.0%; AgNO₃, Fisher, 99.8%; NaNO₃, Fisher, certified ACS grade.

clusters reported in the literature. The silver oxygen distances were slightly longer than those in other compounds with four-coordinate silver. The relative bond lengths of Ag-X, Ag-O, and Na-X indicate that the strongest bonding interaction occurs between silver and the halide, probably because of the relatively strong covalency of the Ag-X bond. Orbital overlap is significant between silver 5s and 5p orbitals and all framework atoms. This means, that although the Ag₄X³⁺ aggregate tends to behave as a unit and can be considered a cluster, it is strongly influenced by the sodalite host.

Another question concerns the interaction of clusters in adjacent cages. Far-IR spectra^{2,39} indicate that cation motions are coupled (mediated by the anions), and anions are also vibrationally coupled (mediated by the cations). This coupling is concentration dependent. Ag-Ag distances between cages were only slightly longer than intracage Ag-Ag separations (25-12% longer than in the corresponding bulk silver halides). With such separations orbital overlap was still significant between cages (highest for Ag 5p levels: 13%). Thus one can expect electronic communication between clusters, resulting in band formation. It is therefore valid to call the arrangement of semiconductor-component clusters an expanded silver halide. One should inquire as to whether it is an expanded semiconductor; AC and DC conductivity measurements on single crystals of silver halosodalites will be required to address this question. Expansion of the semiconductor components and inclusion in a sodalite matrix has increased its energy bandgap compared to the bulk silver halides, as would be expected. The optically determined bandgaps are of the order of 3.8 eV. This value is at the border between semiconductors and insulators.⁹⁵

Another question concerns whether or not the "isolated AgBr molecule" in the NaAgBr-SOD sample with very low silver concentration is fully isolated. The sodium cations, framework atoms, and even bromide ions in adjacent cages still interact with the AgBr diatomic unit, in spite of its short bond length. However, at the low silver loading it is isolated from other AgBr units. This directly affects the optical properties of the material, resulting in more structure in both the absorption and excitation spectra.

Experimental Section

Synthesis of Sodium Sodalite Precursors. The sodium sodalites were prepared by a low temperature hydrothermal synthesis. The gel compositions and the reagent sources are listed in Table IX.

In a typical synthesis, solution A contained the sodium salt, sodium hydroxide, and silica source and solution B contained sodium hydroxide and the alumina source. These were prepared as follows. For solution A, 0.6-zmol of NaOH and wmol of the sodium salt to be occluded in the sodalite were dissolved in 0.6-vmol of deionized water. For class A sodalites an excess of the sodium salt was used to suppress hydroxosodalite formation. An aqueous colloidal silica solution containing ymol of SiO₂ was added to the above solution. The solution was mixed and heated to 80-95 °C. Solution B was prepared by dissolving xmol of Al(OH)₃ in an aqueous solution containing 0.4-zmol of the NaOH, again at 80-95 °C. The hot solutions A and B were mixed rapidly. A gel formed almost immediately upon mixing. The gel was shaken for 5 min, and the mixture was heated at 95 °C for 3-9 days in 1000-mL capped Teflon (FEP) bottles. The white, microcrystalline products were filtered through ASTM 10-15 medium pore glass frits and washed with 2-4 L deionized water. The products were dried in air at ambient temperature.

(93) Burns, G. *Solid State Physics*; Academic Press, Inc.: Orlando FL, 1985.

(94) Berry, C. R. *Phys. Rev.* **1967**, *161*, 848-851.

(95) Strehlow, W. H.; Cook, E. L. *J. Phys. Chem. Ref. Data* **1973**, *2*, 163-193.

Silver Exchange. Melt Exchange. Silver-containing sodalites were prepared by a melt ion exchange of a mixture containing the parent sodium sodalite, AgNO_3 (Fisher, 99.8%), and, in some cases, NaNO_3 (ACS grade) as diluent. Typically, 1–2 g of sodium sodalite was mixed with silver nitrate (mp 212 °C)⁹⁶ in a porcelain mortar. For complete silver exchange a slight excess of silver nitrate was used, while for partial exchanges stoichiometric amounts were used. The mixture was heated in the dark to 230 °C for 24 h (320 °C if NaNO_3 was used). For milder exchange conditions, a eutectic mixture containing 50 wt% AgNO_3 and 50 wt% AgClO_3 can be used. Its eutectic melt temperature is 145 °C.⁹⁷ The products were filtered in the dark through a 0.8 μm cellulose nitrate filter membrane, washed with ca. 2 L of deionized water, and dried in air at ambient temperature. Because of their light sensitivity, the white-to-yellow dry powders were stored in dark sample vials.

Aqueous Exchange. An aqueous ion exchange is possible for even milder exchange temperatures (room temperature up to 100 °C). Sodium sodalite was added to an aqueous solution containing stoichiometric amounts of silver nitrate. The mixture was stirred in the dark for 24 h at room temperature or under reflux. The product was filtered, washed in the dark, and dried in air. For halosodalites only partial silver exchange was accomplished, even under reflux conditions.

Product Characterization. Sample Preparation. For many spectroscopic investigations samples were pressed into 20-mm diameter self-supporting wafers with a pressure of ca. 200 MPa for 2 s. With careful grinding, the sodalite crystal structure was not significantly reduced by this procedure. Multiple grinding and pressing, however, led to degradation of the crystallinity. Some silver sodalites proved to be pressure sensitive and darkened upon compression.

All thermal manipulations were carried out in situ, using standard high-vacuum techniques. Analyses were usually carried out at or near room temperature.

Powder X-ray Diffraction (XRD). The products from the hydrothermal syntheses and silver exchanges were analyzed by powder X-ray diffraction. Samples were prepared by spreading a thin layer of finely ground sodalite on an etched glass or plexiglass slide, with a 0.3–3 mm square groove.

Room-temperature (25 °C), high resolution powder X-ray data were collected on a Scintag PAD-X automated diffractometer operating in θ - θ geometry, using $\text{Cu K}\alpha$ radiation ($\lambda = 1.54178 \text{ \AA}$, $K\alpha_2$ stripped, 40 mA, 45 kV) with a liquid nitrogen cooled solid state Ge detector. A scan range from $2\theta = 15$ – 80° in 0.01° steps was used for a total of 6500 data points, allowing for the collection of a pattern with sufficient intensity (signal:noise) within ca. 12–14 h. The Scintag equipment was interfaced with a Digital Corp. Microvax II computer, running associated software. Lattice indexing, unit cell size determination and esd calculations were carried out using Scintag software modified at the University of California, Santa Barbara.

The Rietveld refinements were carried out using the program GSAS¹² on a Microvax II computer. For each refinement the space group $P43n$ was used, assuming a random distribution of cages occupied by different guest species. The general positions and fractional occupancies of the cations, anions, and framework oxygens were refined. The temperature factors were generally refined isotropically (not refined for framework Si, Al).

Product Composition. The sodalite samples were analyzed for Si, Al, Na, Ag, Br, Fe, and Pb by Galbraith Laboratories, Knoxville, TN. Table III lists the compositions of the sodalites that were chemically analyzed. The compositions of the sodium sodalites were consistent with the expected sodalite structure. The Si/Al ratios of all samples fell in the range from 1.03–1.11, as expected for a well-ordered sodalite. The XRD powder patterns showed one major sodalite phase. A relatively flat background indicated that not much amorphous material was present. The line width of the X-ray lines was typical for hydrothermally prepared sodalites with small particle size. Single phases were observed, except in a few samples which were partially dehydrated and could therefore exhibit patterns corresponding to regions of different states of hydration. No lines due to externally crystallized sodium halides or silver were observed for the untreated materials.

The halide content of NaBr-SOD and its silver derivatives was found to be 6–19% lower than expected in a perfect material, indicating that some cages were created with trapped hydroxide (or no anion after washing) or that small amounts of amorphous material free of halide was present. Hydroxide or anion-free "defect" cages were detected directly by ^{23}Na MAS-NMR.²

Fourier Transform Infrared (FT-IR) Spectroscopy. Infrared measurements were carried out on a Nicolet 20SXB Fourier Transform IR

spectrometer with far infrared capability (Nicolet 20F, 650–30 cm^{-1} , DTGS detectors). All spectra were obtained with 4 cm^{-1} resolution by co-adding 250 interferograms (650–30 cm^{-1} far IR range) or 100 interferograms (4000–400 cm^{-1} mid IR range). The spectra were baseline-corrected by subtracting a linear ramp from the observed spectra. Some mid-IR spectra were collected on a Nicolet DX5 FT spectrometer. As sodalites absorb strongly in the IR framework region, samples were diluted with CsCl or KBr for mid-IR analysis to resolve individual framework bands. Self-supporting wafers were prepared by pressing a few grains of sodalite mixed with the salt. Since only milligram quantities were used, care had to be taken that the sample was representative of the bulk material.

For far-IR measurements the sodalites were treated in an in situ cell.⁴⁸ Around 20–50 mg of sodalite powder was diluted with an equal amount of dry silica gel (ICI: Davison 952) to improve wafer stability and conserve sample, and formed into 20-mm diameter self-supporting wafers. Up to four wafers were mounted in a sample holder that could be rotated through 360° as well as vertically translated in a dynamic vacuum. The zeolite wafers were moved either to intersect the IR beam or to a water-cooled furnace area for thermal treatments. The wafers could be heated in the IR beam by a cartridge heater embedded into the sample holder or moved to the furnace area where it was possible to attain temperatures up to 450 °C for pre- or post-treatment in a dynamic vacuum of 10^{-6} Torr. Samples could be cooled to ca. –50 °C by passing liquid nitrogen-cooled dry nitrogen gas through a coil attached to the sample holder.

Solid State Nuclear Magnetic Resonance (NMR) Spectroscopy. ^{27}Al , ^{29}Si , ^{23}Na MAS-NMR measurements at 7.0 T were carried out on a General Electric GN-300 spectrometer at the University of California, Santa Barbara, equipped with Henry-Radio amplifiers and a Chemagnetics probe. MAS-NMR experiments were conducted using KELEF rotors of 9.5 mm o.d. which were spun at speeds up to 3.5 kHz.

The spectra were recorded, using the following conditions: ^{29}Si , 59.7 MHz; pw = 7–15 μs ; pd = 120 s; csr, TMS; ^{27}Al , 78.3 MHz; pw = 8–15 μs ; pd = 2 s; csr, 1 M $\text{Al}(\text{NO}_3)_3$ aqueous solution; ^{23}Na , 79.5 MHz; pw = 2–15 μs ; pd = 1–2 s; csr, solid NaCl. (Here pw = pulse width, pd = pulse delay, csr = chemical shift reference. The chemical shift of solid NaCl is 7.9 ppm with respect to 1 M NaCl aqueous solution.⁶¹)

In addition ^{23}Na MAS-NMR measurements at 7.0 T were carried out at the University of Toronto, using a Chemagnetics CMX-300 spectrometer with Chemagnetics MAS probe and rotor and 7.5 mm zirconia spinners at speeds of ca. 3 kHz. The following conditions were used: ^{29}Si , 59.5 MHz; pw = 5 μs ; pd = 120 s; csr, TMS. ^{23}Na , 79.2 MHz; pw = 2 μs ; pd = 2 s; csr, solid NaCl.

^{23}Na and ^{27}Al DOR experiments were conducted on a 11.7 T Chemagnetics CMX-500 spectrometer at the University of California, Berkeley equipped with a DOR probe. The outer rotor spinning rate was 500–650 Hz, and the inner rotor spinning rate was 5 kHz. The following experimental parameters were used: ^{27}Al , 130.3 MHz; pw = 3 μs ; pd = 0.5–1 s; csr, dilute aqueous $\text{Al}(\text{NO}_3)_3$ solution; ^{23}Na , 132.3 MHz; pw = 4 μs ; pd = 0.5 s; csr, 1 M aqueous NaCl solution.

Optical Spectroscopy. UV-visible absorption spectra were obtained by a reflectance method, using a Perkin Elmer 330 spectrophotometer with an integrating sphere (BaSO_4 reference) and a range of 190–2400 nm. Samples were pressed into self-supporting pellets. The spectrometer reports $\log(1/R_\infty)$ versus wavelength, where R_∞ is the relative diffuse reflectance, defined by

$$R_\infty = \frac{R'_s \text{ sample}}{R'_s \text{ reference}}$$

R'_s is the absolute reflectance of the layer, k its molar absorption coefficient, and s the scattering coefficient. (The k values for the BaSO_4 reference are assumed to be zero and its absolute reflectance to be one.)

In order to determine bandedges, spectra were first converted from reflectance to absorption units using the Kubelka-Munk equation. The theory concerning diffuse reflectance spectroscopy has been developed by Kubelka and Munk^{98,99} and is outlined by Frei and MacNeil.^{100,101} The bandedges were then fitted to the corrected spectra using equations for direct and indirect bandgap semiconductors.³³ The energy gaps were calculated by plotting α^2 , $\alpha^{2/3}$, $\alpha^{1/2}$, or $\alpha^{1/3}$ versus the absorption energy for da , df , ia , and if interband transitions, respectively. The intersection of the extrapolated best fitting straight line with the horizontal (energy)

(98) Kubelka, P.; Munk, F. *Z. Tech. Phys.* 1931, 12, 593.

(99) Kubelka, P. *J. Opt. Soc. Am.* 1948, 38, 448.

(100) Frei, R. W.; MacNeil, J. D. *Diffuse Reflectance Spectroscopy in Environmental Problem Solving*; CRC Press: Cleveland, OH, 1973.

(101) Bohren, C. F.; Huffman, D. R. *Absorption and Scattering of Light by Small Particles*; J. Wiley & Sons: New York, 1983; p 132.

(96) *CRC Handbook of Chemistry and Physics*, 61st ed.; Weast, R. C., Ed.; CRC Press, Inc.: Boca Raton, FL, 1980.

(97) Phillips, M., private communication.

axis (i.e., extrapolation to $\alpha = 0$) was taken as the bandgap energy.

When $\hbar\omega \geq E_g + \hbar\omega_c$ then $\alpha_{ia} = \alpha_{ia}^a + \alpha_{ia}^c$.^{85,93} Plots of $\alpha^{1/2}$ versus $\hbar\omega$ (or $\hbar\nu$) should have two straight line portions which extrapolate to $E_g + \hbar\omega_c$ and $E_g - \hbar\omega_c$. Changes in temperature change the relative contributions of phonon absorption and emission as well as the value of E_g because of changes in the lattice constant.

EHMO Calculations. Extended Hückel molecular orbital (EHMO) calculations were carried out for silver and silver halide clusters, in the free form as well as enclosed in a sodalite cage. The program ICONCL by Calzaferri and co-workers¹⁰² was used for this calculation. This program is based on the Mulliken–Wolfsberg–Helmholz method.¹⁰³ The orbital exponents were taken from available literature data.^{104–106} The Coulomb integrals used were those of the neutral atoms (except for Ag^+ , where the values for the +1 ion were used). These values were obtained from the literature.^{107–109} In some calculations, self-consistent charge iterations were carried out for Ag, Cl, Na, Si, Al, and O, to optimize the Coulomb integrals using the equation

$$-H_{ii}(Q) = AQ^2 + BQ + C$$

with parameters A, B, and C based on literature values.^{103,107–109}

The resonance integrals were calculated using the Wolfsberg–Helmholz equation with Calzaferri's distance dependent term^{83,84}

$$H_{ij} = k \frac{S_{ij}}{2} (H_{ii} + H_{jj})$$

where $k = 1 + (\kappa + \Delta^2 - \Delta^4\kappa) \cdot \exp[-\delta(R - d_0)]$, $d_0 = r(\text{A}) + r(\text{B})$, $1 + \kappa = 2.0$, $\delta = 0.35$ (recommended values for inorganic complexes), and $\Delta = H_{ii} - H_{jj}/H_{ii} + H_{jj}$.

The equation takes into account the difference in diffuseness of orbitals, assuming that a small H_{ij} implies an unstable, diffuse orbital and a large H_{ii} a stable, contracted orbital.

(102) Calzaferri, G.; Forss, L.; Hugentobler, T.; Kamber, I. *ICONCL and INPUTC*, Fortran software for extended Hückel molecular orbital calculations, Institute for Inorganic and Physical Chemistry, University of Bern, Freiestrasse 3, CH-3009 Bern, 1989.

(103) McGlynn, S. P.; Vanquickenborne, L. G.; Kinoshita, M.; Carroll, D. G. *Introduction to Applied Quantum Chemistry*; Holt, Rinehart and Winston, Inc.: New York, 1972.

(104) Clementi, E.; Roetti, C. *Atomic Data Nuclear Data Tables* **1974**, *14*, 177–478.

(105) Fitzpatrick, N. J.; Murphy, G. H. *Inorg. Chim. Acta* **1984**, *87*, 41–46.

(106) Fitzpatrick, N. J.; Murphy, G. H. *Inorg. Chim. Acta* **1986**, *111*, 139–140.

(107) Basch, H.; Viste, A.; Gray, H. B. *Theor. Chim. Acta (Berlin)* **1965**, *3*, 458–464.

(108) Basch, H.; Gray, H. B. *Theor. Chim. Acta (Berlin)* **1966**, *4*, 367–376.

(109) Baranovskii, V. I.; Nikol'skii, A. B. *Teoreticheskaya i Eksperimental'naya Khimiya* **1967**, *3*, 527–533.

(110) Meier, W. M.; Olson, D. H. *Atlas of Zeolite Structure Types*; Structure Commission of the International Zeolite Association, 1978; p 81.

(111) Norby, P.; Norlund Christensen, A.; Krogh Andersen, I. G. *Acta Chem. Scand.* **1986**, *A40*, 500–506.

(112) Johnsson, M.; Persson, I. *Inorg. Chim. Acta* **1987**, *130*, 215–220.

(113) Holmberg, B.; Johansson, G. *Acta Chem. Scand.* **1983**, *A37*, 367–381.

(114) Dalba, G.; Fornasini, P.; Rocca, F. J. *Non-Cryst. Solids* **1990**, *123*, 310–314.

The above method uses all valence electrons but neglects inner shell electrons. Antisymmetrization and electron correlation are also neglected. Even though it uses the simplest of all valence one-electron theories, it was considered suitable for the systems studied here, because it can handle relatively complex inorganic, nonplanar systems, providing a reasonable qualitative picture of the electronic structure.

Acknowledgment. We acknowledge the Natural Science and Engineering Research Council (N.S.E.R.C.) of Canada's Operating (G.A.O.), P.M.M) and Strategic Grants Programmes, Alcan Canada and Optical Recording Corporation, Toronto (G.A.O.); Office of Naval Research and the National Science Foundation (QUEST), (G.D.S.); and Director, Office of Energy Research, Office of Basic Energy Sciences, Materials Sciences Division, U.S. Department of Energy under contract No. DE-AC03-76SF00098 (R.J.) for generous financial support of this work. A.S. thanks N.S.E.R.C. for a 1967 Science and Engineering Postgraduate Scholarship. We thank Alan Benesi, Jürgen Plischke, Albert Vannice, Bill Harrison, Nancy Keder, James MacDougall, Alexander Pines and Bill Mercer for valuable technical assistance and discussions.

Registry No. $\text{Na}_{5.3}\text{Ag}_{2.4}\text{Br-SOD}$, 141017-47-2; $\text{Na}_{5.5}\text{Ag}_{2.5}\text{Br-SOD}$, 141017-31-4; $\text{Na}_{7.6}\text{Ag}_{0.3}\text{Br-SOD}$, 141017-51-8; $\text{Na}_{7.7}\text{Ag}_{0.3}\text{Br-SOD}$, 141017-30-3; $\text{Al}_{5.9}\text{Na}_{7.5}\text{Br}_{1.82}(\text{OH})_{3.23}\text{O}_{3.98}(\text{SiO}_3)_{6.1}$, 141017-53-0; $\text{Al}_{5.88}\text{Ag}_{0.05}\text{Na}_{7.7}\text{Br}_{1.75}(\text{OH})_{4.23}\text{O}_{3.57}(\text{SiO}_3)_{6.12}$, 141017-52-9; $\text{Al}_{5.87}\text{Ag}_{0.68}\text{Na}_{7.17}\text{Br}_{1.72}(\text{OH})_{9.68}\text{O}_{0.91}(\text{SiO}_3)_{6.13}$, 141017-50-7; $\text{Al}_{5.86}\text{Ag}_{1.27}\text{Na}_{6.57}\text{Br}_{1.74}(\text{OH})_{7.03}\text{O}_{2.19}(\text{SiO}_3)_{6.14}$, 141017-49-4; $\text{Al}_{5.83}\text{Ag}_{2.01}\text{Na}_{6.09}\text{Br}_{1.78}(\text{OH})_{5.08}\text{O}_{3.18}(\text{SiO}_3)_{6.17}$, 141017-48-3; $\text{Al}_{5.78}\text{Ag}_{3.05}\text{Na}_{4.61}\text{Br}_{1.65}(\text{OH})_{10.92}(\text{SiO}_3)_{6.22}$, 141017-42-7; $\text{Al}_{5.73}\text{Ag}_{3.88}\text{Na}_{3.97}\text{Br}_{1.62}(\text{OH})_{7.78}\text{O}_{1.54}(\text{SiO}_3)_{6.27}$, 141017-46-1; $\text{Al}_{5.72}\text{Ag}_{4.65}\text{Na}_{3.41}\text{Br}_{1.67}(\text{OH})_{5.41}\text{O}_{2.79}(\text{SiO}_3)_{6.28}$, 141017-45-0; $\text{Al}_{5.7}\text{Ag}_{5.66}\text{Na}_{2.78}\text{Br}_{1.88}(\text{OH})_{7.92}\text{O}_{1.56}(\text{SiO}_3)_{6.3}$, 141017-44-9; $\text{Al}_{5.73}\text{Ag}_{8.45}\text{Na}_{0.03}\text{Br}_{1.81}(\text{OH})_{2.86}\text{O}_{4.22}(\text{SiO}_3)_{6.27}$, 141017-43-8; $\text{Na}_8\text{Cl}_2(\text{SiAlO}_4)_6$, 12336-79-7; $\text{Ag}_8\text{Cl}_2(\text{SiAlO}_4)_6$, 141017-32-5; $\text{Na}_8\text{I}_2(\text{SiAlO}_4)_6$, 53238-78-1; $\text{Ag}_8\text{I}_2(\text{SiAlO}_4)_6$, 82641-93-8; $\text{Na}_{7.9}\text{Ag}_{0.1}\text{Cl}_2(\text{SiAlO}_4)_6$, 141017-39-2; $\text{Na}_7\text{AgCl}_2(\text{SiAlO}_4)_6$, 141017-40-5; $\text{Na}_4\text{Ag}_4\text{Cl}_2(\text{SiAlO}_4)_6$, 141017-41-6; $\text{Na}_{7.9}\text{Ag}_{0.1}\text{I}_2(\text{SiAlO}_4)_6$, 141017-36-9; $\text{Na}_7\text{AgI}_2(\text{SiAlO}_4)_6$, 141017-37-0; $\text{Na}_4\text{Ag}_4\text{I}_2(\text{SiAlO}_4)_6$, 141017-38-1; $\text{Al}(\text{OH})_3$, 21645-51-2; SiO_2 , 7631-86-9; NaOH , 1310-73-2; NaCl , 7647-14-5; NaBr , 7647-15-6; NaI , 7681-82-5; AgNO_3 , 7761-88-8; NaNO_3 , 7631-99-4; $\text{Na}_4\text{Cl}^{3+}$, 140677-25-4; $\text{Na}_3\text{AgCl}^{3+}$, 140677-26-5; $\text{Na}_2\text{Ag}_2\text{Cl}^{3+}$, 140677-27-6; $\text{NaAg}_3\text{Cl}^{3+}$, 140677-28-7; $\text{Ag}_4\text{Cl}^{3+}$, 140677-29-8; $\text{Al}_{12}\text{Si}_{12}\text{O}_{36}^{12+}$, 140677-30-1; $\text{Ag}_8\text{Cl}_2\text{Al}_{12}\text{Si}_{12}\text{O}_{36}^{18+}$, 141017-35-8; $\text{Ag}_{16}\text{Cl}_4\text{Al}_{12}\text{Si}_{12}\text{O}_{36}^{24+}$, 141017-34-7.

Supplementary Material Available: Crystallographic data for NaBr-SOD , $\text{Na}_{7.6}\text{Ag}_{0.3}\text{Br-SOD}$, $\text{Na}_{5.3}\text{Ag}_{2.4}\text{Br-SOD}$, AgBr-SOD , $\text{Na}_8\text{Br}_{0.26}[\]_{1.74}\text{-SOD}$, $\text{Ag}_8\text{Br}_{0.26}[\]_{1.74}\text{-SOD}$, $\text{Ag}_8\text{Br}_{0.46}[\]_{1.54}\text{-SOD}$, $\text{Ag}_8\text{Br}_{1.18}[\]_{0.82}\text{-SOD}$, class A sodalite structural parameters, Ag-O , Ag-Br , and Ag-Ag structural data related to class A silver halosodalites, and class A sodalite compositions (11 pages). Ordering information is given on any current masthead page.

(115) Dallinga, G.; Mackor, E. L. *Recl. Trav. Chim. Pays-Bas* **1956**, *75*, 796–801.

(116) Jelinek, R.; Ozin, G. A.; Stein, A. *J. Phys. Chem.*, in press.